# HOMOCLINIC ORBITS IN THE COMPLEX DOMAIN


V.F.Lazutkin[1] and C.Simó[2]

[1] St.-Petersburg State University,
[2] Universitat de Barcelona



Abstract

We consider the standard map, as a paradigm of area preserving map, when the variables are taken as complex. We study how to detect the complex homoclinic points, which can not dissappear under a homoclinic tangency. This seems a promising tool to understand the stochastic zones of area preserving maps. The paper is mainly phenomenological and includes theoretical support to the observed phenomena. Several conjectures are stated.



AMS Subject Classification: 58F05


## 1. Introduction

We start with the following picture (see figure 1) which represents several orbits of the map

$$\begin{pmatrix} x \\ y \end{pmatrix} \mapsto \begin{pmatrix} 0.2\cos 2\pi x - y \\ x \end{pmatrix} \tag{1}$$

defined on the 2-torus $\mathbb{T}^2 = \mathbb{R}^2/\mathbb{Z}^2$. Only one quarter of the torus, namely the domain $|x| \le 1/4$, $|y| \le 1/4$, is drawn. The remaining part can be restored by symmetry. The map in $\mathbb{T}^2$ is invariant under the symmetry $S:(x,y)\mapsto(\frac12 - x, \frac12 - y)$. It has two elliptic points $(x^*,x^*)$ and $(\frac12 - x^*, \frac12 - x^*)$, where $x^*$ is the first positive solution of $2x = 0.2\cos 2\pi x$. The points $(x^*+\frac12, -x^*)$ and $(-x^*, x^*+\frac12)$ are an elliptic period 2 orbit. The points $(\pm\frac14, \pm\frac14)$ are an hyperbolic period 4 orbit. One can also reduce (via symmetry) the phase space and consider this picture as the whole phase space, the edges being glued by the maps $(-\frac14, y)\mapsto(\frac14, -y)$ and $(x, -\frac14)\mapsto(-x, \frac14)$. The resulting surface is a projective plane with two singular points which correspond to the corners (an orbifold with two $\mathbb{Z}_2$-points).

This is a typical picture of the phase space of an area-preserving map. One can see an elliptic fixed point surrounded by KAM curves, each bearing a quasiperiodic motion, a chain of islands of period 7 on the periphery of the set of KAM curves (they also consist of KAM curves), and a "stochastic zone". The latter is the most mysterious component of the phase space. The common belief is that this zone has positive area, and the Lyapunov exponents are positive at points belonging to it. So it is a natural object of Pesin's theory [Pes1]: the dynamics of the map,


Typeset by $\mathcal{A}\mathcal{M}\mathcal{S}$-TEX

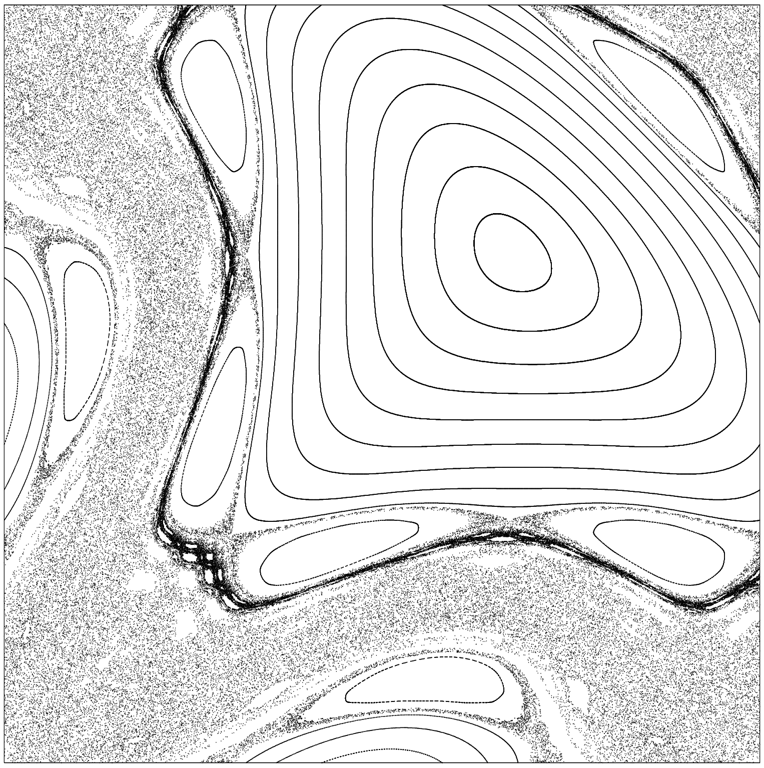

**Figure 1.** The phase portrait of system (1) on the projective plane $|x| \leq 1/4, |y| \leq 1/4$. Several trajectories are drawn representing all the characteristic features of the system.

restricted to it, is modelled by a Bernoulli process with a finite number of states. The difficulty is that there is a lot of chains of (very thin) islands with very high periods. They can be visible only after a very big zoom. The islands are extremely deformed. Such islands pervade densely the stochastic zone, and the area of the latter equals to the visible area minus the sum of the areas of the islands.

Analogously, if one explores thoroughly the part of the phase space occupied by KAM circles, one finds other small stochastic zones in the gaps between KAM circles, the thin stochastic zones also pervading the phase space densely.

There are many approaches in trying to understand this "stochastic zone". The one we are going to develop here is the complex approach. It comes from a general philosophy which tells us: *each item in the real domain has its counterpart in the complex domain, its complexification, or its analytic continuation. To understand completely the item, one has to investigate its complexification. A general law is that the complex things look simplier than their real prototypes.* We are going to look at the chaotic zone from the complex point of view. How does it look like, and what it might be? Of course, the map itself is analytic and has a unique analytic extension, and we have to explore that extension, its orbits etc. The main tool to approach the problem in this paper will be a numerical simulation accompanied by theoretical speculations about the geometric an analytical nature of the objects which arise in the process of exploration.

## 2. Basic concepts

Let us dwell on the initial concepts. Let $S$ be a surface, *i.e.*, a 2-dimensional manifold, equipped with an area form $\Omega$, and let $F\colon S \to S$ be a map which preserves $\Omega$, that is $F^*\Omega = \Omega$. All maps and manifolds are supposed to be real analytic. A basic example (see [Ch]) is the so called *standard map*, $SM\colon \mathbb{T}^2 \to \mathbb{T}^2$, which is defined on the 2-torus $\mathbb{T}^2 = \mathbb{R}^2/2\pi\mathbb{Z}^2$ equipped with the standard area form $\Omega = dx \wedge dy$. The map itself is given by the formulae:

$$\begin{aligned} SM(x,y) &= (x_1, y_1)\,, \\ x_1 &= x + y_1\,, \\ y_1 &= y + \varepsilon \sin x\,. \end{aligned} \tag{2}$$

Most of pictures that we are going to present here come from numerical experiments with the SM.

A point $p \in S$ is called a *fixed point* for the map $F$ if $F(p) = p$. A fixed point $p$ is *hyperbolic* if the tangent map, $F'(p)$, represented as a $2{\times}2$ -matrix in local coordinates, has the spectrum which does not intersect with the unit circle in the complex domain. In that case, the matrix of $F'(p)$ in appropriate coordinates reads

$$\begin{pmatrix} \lambda & 0 \\ 0 & \lambda^{-1} \end{pmatrix}, \qquad |\lambda| > 1\,, \tag{3}$$

where $\lambda$ is real for the real map. For example, the SM has $(0,0)$ as a hyperbolic fixed point, the largest eigenvalue of (3) being

$$\lambda = \lambda(\varepsilon) = 1 + \frac{1}{2}\varepsilon + \sqrt{\varepsilon + \frac{1}{4}\varepsilon^2}\,. \tag{4}$$

It is a well known fact that any hyperbolic fixed point $p$ (more generally, a hyperbolic periodic trajectory) possesses *stable*, $W^s(p)$, and *unstable*, $W^u(p)$, manifolds. Both are injectively immersed 1-dimensional manifolds (curves) passing through $p$, the tangent directions to $W^{s,u}(p)$ at $p$ coinciding with the eigendirections of $F'(p)$ corresponding to $\lambda^{-1}$ and $\lambda$, respectively.

The stable and unstable manifolds of a hyperbolic fixed point $p$ can possess other intersections apart from $p$ itself. They are called *homoclinic* points. The existence of homoclinic points leads to a very complicated behaviour of the iterates of the map and serves as a source of stochastization. Once a homoclinic point is available, there exist many of them. Henri Poincaré in his famous book "Les méthodes nouvelles de la méchanique céleste" described the situation in the following words:

"When we try to represent the figure formed by these two curves and their infinitely many intersections, each corresponding to a doubly asymptotic solution, these intersections form a type of trellis, tissue, or grid with infinitely fine mesh. Neither of the two curves must ever cut across itself again, but it must bend back upon itself in very complex manner in order to cut across all the meshes in the grid an infinite numbers of times.

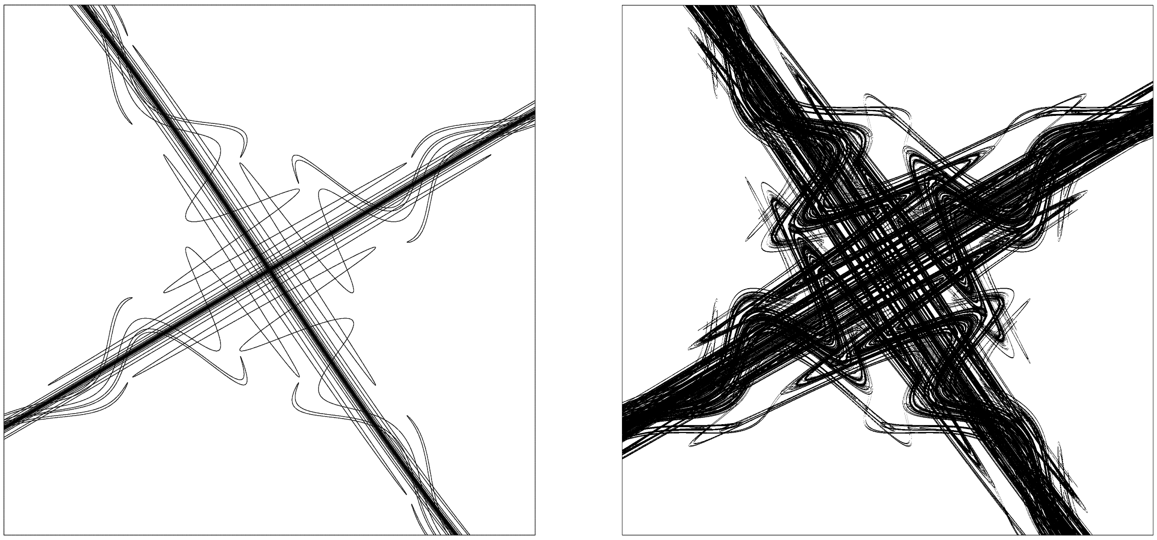

*a*) *b*)

**Figure 2.** Several homoclinic intersections near a fixed point of the SM in the real domain: The homoclinic trellis. An illustration to the citation from Poincaré book. $\varepsilon = 0.9$. Window: $[-1,1]\times[-1,1]$. See additional explanations in the text.

The complexity of this figure is striking, and I shall not even try to draw it. Nothing is more suitable for providing us with an idea of the complex nature of three-body problem, and of all problems of dynamics in general, where there is no uniform integral and where the Bohlin series are divergent" [Po, Part 3, p.1059].

A part of the picture, which Poincaré did not dare to draw, made by computer in a neigbourhood of the fixed hyperbolic point of the standard map, is shown in figure 2.

Only finite (and not very long) parts of the stable and unstable manifolds are drawn on figure 2. In both cases, *a*) and *b*), a local expansion of the unstable manifold using (5) (see below) up to order 50 has been used to obtain one branch of $W^u$. Then a suitable fundamental domain is iterated several times (i.e., we are using formulas (7) and (8)), with changing step size to follow the manifold faithfully (see [S]). The other branch is obtained by symmetry, and the stable manifold by using the reversor $R$ given in (13). The arc lenght, counted from the fixed point, is of 100 units in *a*) and 10,000 units in *b*). If we prolong $W^s$ and $W^u$ infinitely, the picture will look like figure 3. This picture has been obtained by taking 1,000 points in a fundamental domain (going up to $\xi = 1$, see (5)) and by iterating each of them 100,000 times. Notice, however, that during the iteration the errors increase, and they occur, essentially, along the direction of $W^u$. Hence, by iteration of only one point in $W^u$ for a sufficiently large number of times, the figure appears to be the same. We note also that figure 2 *a*) (resp. 2 *b*)) is equivalent to only 13 (resp. 24) iterations of the same fundamental domain.

One can see specific features of the stochastic area observed on figure 1. The conclusion is that the complicated behaviour of $W^s$ and $W^u$ creates the stochastic zones.

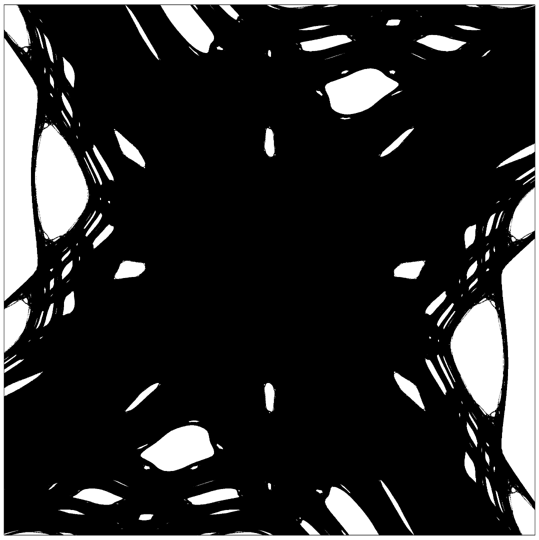

**Figure 3.** The same as in figure 2 but with infinite (= very large) number of iterates. Window: $[-1,1]\times[-1,1]$. See additional explanations in the text.

This observation gives us a clue to the question posed at the beginning of the paper: what is a complex continuation of the stochastic zone. Since the latter is created, in some sense, by the stable and unstable manifolds of a hyperbolic fixed point, one can try to continue analytically those stable and unstable manifolds and look at the figure they create there. Special attention has to be payed to the intersections of $W^s$ and $W^u$ which appear in the complex domain, the *complex homoclinic points.*

When trying to fulfill this program, one encounters the following two difficulties:

(1) How to do numerically an analytical continuation of $W^s$ and $W^u$ ?
(2) How to find numerically complex homoclinic points ?

## 3. Computation of invariant manifolds

We assume that the map $F\colon S\to S$ has an analytic extension onto a *complexified phase space,* $S^{\mathbb{C}}$, of the real phase space $S$, keeping the same notation, $F$, for the extended map. In the case of the SM, the complexified phase space is $\mathbb{C}^2/2\pi\mathbb{Z}^2$ and the prolonged SM is given by the same expressions (2), the variables $x$ and $y$ ranging now in the complex domain.

The first difficulty can be overcome via the following procedure which consists of two steps.

Step 1. To find $W^u_{loc}(p)$, a small piece of $W^u(p)$ in a vicinity of $p$, the fixed hyperbolic point, choose a suitable coordinate system, $(x,y)$, such that $(0,0)$ corresponds to $p$, and use the Taylor expansion

$$\begin{pmatrix} x \\ y \end{pmatrix} = \begin{pmatrix} x(\xi) \\ y(\xi) \end{pmatrix} = \sum_{k=1}^{\infty} \begin{pmatrix} a_k \\ b_k \end{pmatrix} \xi^k , \tag{5}$$

subjecting the variable $\xi$, a coordinate along $W^u_{loc}(p)$, to the following condition: the restriction of $F$ onto $W^u_{loc}(p)$ reads, in terms of $\xi$:

$$\xi \longmapsto \lambda\xi \,, \tag{6}$$

$\lambda$ being the largest eigenvalue of $F'(p)$ (see the formula (3)). The condition (6) defines the variable $\xi$ uniquely, up to a nonzero multiplier. It follows from Moser's theorem [Mo] that the series (5) converges in a neighbourhood of $\xi = 0$. In fact, for the SM, the series (5) converges for all $\xi \in \mathbb{C}$. Technical details concerning the computation of the coefficients $a_k$, $b_k$, can be found in [GLST]. The expansion has been normalized, in the case of the SM, by taking $a_1 = 4$. In any way, one can use (5) for the numerical calculation of the analytical continuation of $W^u$ in the complex domain, taking the values of $\xi$ in a disk $D_0$ around 0 in $\mathbb{C}$ of small radius, $\delta$. The formula (5) defines an analytic map $\Phi_{loc}\colon D_0 \to S^{\mathbb{C}}$.

Step 2. To find the global unstable manifold, $W^u(p)$, apply the iterates of the map $F$ to points of $W^u_{loc}(p)$:

$$W^u(p) = \bigcup_{n=0}^{\infty} F^n \left(W^u_{loc}(p)\right) \,. \tag{7}$$

Thus, the manifold $W^u(p)$ is the image of $\mathbb{C}$ under an analytic injective immersion $\Phi\colon \mathbb{C} \to S^{\mathbb{C}}$ given by the formula

$$\Phi(\xi) = F^n \circ \Phi_{loc}(\lambda^{-n}\xi)\,, \quad \lambda^{-n}\xi \in D_0 \,. \tag{8}$$

## 4. Ferns

Let us discuss the second difficulty. How to recognize a homoclinic point on $W^u(p)$?

To observe homoclinic points, one can use the coordinate $\xi$ introduced by the formulae (5), (6). Each homoclinic trajectory intersects each domain of the form $C\lambda^{-1} \le |\xi| < C$ exactly at a single point. Hence, we can restrict ourselves to consider the domain $D_0 \setminus \left(\lambda^{-1} D_0\right)$. In the case of the SM, the symmetry reasons enable us to consider only one quarter of the fundamental domain. The change of coordinate

$$\xi \longmapsto z = \frac{\log \xi}{\log \lambda} \tag{9}$$

converts the said quarter to a rectangle

$$D = \left\{ z \in \mathbb{C}\colon\ z_0 - 1 \le |\mathrm{Re}\, z| < z_0 \,,\ 0 \le \mathrm{Im}\, z \le \frac{\pi}{2\log\lambda} \right\} , \tag{10}$$

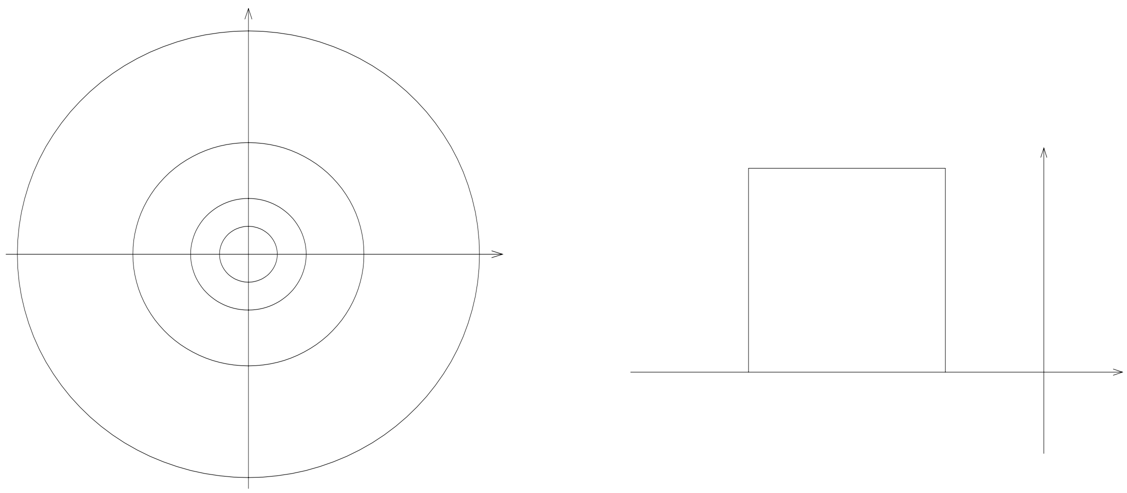

*a*) *b*)

**Figure 4.** *a*) A part of the plane of the variable $\xi$ with several annuli (the fundamental domains) and with $D_0$. *b*) The domain $D$ in the plane $z$ (see formula (10)).

where $z_0 = \frac{\log \delta}{\log \lambda}$ (see figure 4).

A point $q \in W^u(p)$ can be parametrized (up to a simple symmetry transformation) by a point $z \in D$, and an integer $n$ such that $\Phi^{-1}(q) \in \lambda^n D_0$. Denote by $\Psi : D \to S^{\mathbb{C}}$ the composition of the inverse of the map given by (9) and the map $\Phi$ introduced in (8).

How to recognize a homoclinic point in $D$? In [GLST] we found experimentally a test which permits to identify at least some of the complex homoclinic points. The experiments were made for the SM given by the equations (2) mainly with $\varepsilon = 0.5$, but other values of $\varepsilon$ were also considered. We classified points $z \in D$ according to the behaviour of the iterates of $\Psi(z)$ in the forward direction. If the imaginary part of the first component of $F^n(\Psi(z))$ remains positive for all positive $n$, and tends to $+\infty$, as $n \to +\infty$, we marked the point $z$ in black. Otherwise $z$ is coded in white. We say that these points have zero jumps, because, along the orbit, $\operatorname{Im} x$ has not "jumped" to negative values before escaping.

In such a way we obtained the picture drawn on figure 11 of [GLST], which displayed a fractal structure called "ferns". We reproduce this picture in figure 5.

In fact we draw black or white a pixel on figure 5, $z$ being the center of the pixel. In figure 5, as well as in other figures displaying ferns of the SM, the variable $z$ has been slightly modified to a new variable $\hat{z}$ by keeping the same real part and multiplying the imaginary part by $\frac{2 \log \lambda(\varepsilon)}{\pi}$. In this way the domain of $\hat{z}$, corresponding to one quarter of a fundamental domain of the $W^u$ of the SM, is the square $[-1, 0] \times [0, 1]$, independently of the value of $\varepsilon$.

Furthermore, from a practical point of view, some remarks must be made.

(1) The escape criterion has been taken as follows: A point is considered as escaping if $|\operatorname{Im} x| > M$ for some value of $M$. As the next iterate requires the

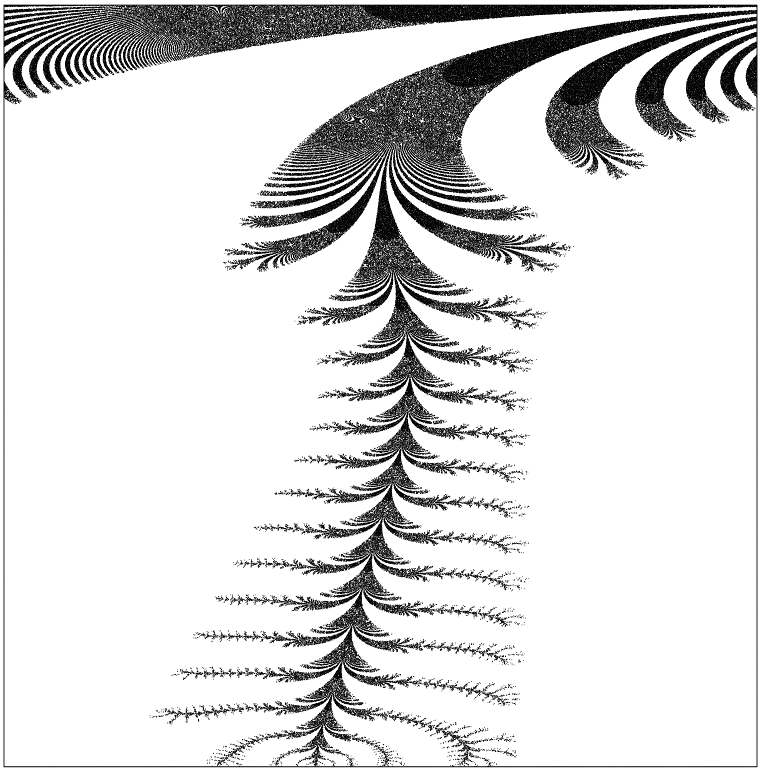

**Figure 5.** The fern corresponding to zero jumps for $\varepsilon = 0.5$. Domain of the $\hat{z}$ variable: $[-1,0] \times [0,1]$.

computation of the functions $\cosh(\mathrm{Im}\, x)$ and $\sinh(\mathrm{Im}\, x)$, we must prevent from overflow in this part. Typically the value $M = 700$ has been used when working in double precision arithmetics and $M = 11300$ in quadruple one. Therefore, in principle, as soon as $|\mathrm{Im}\, x| > M$ a pixel would be marked black. When increasing $M$ the number of points marked black decreases (to zero if exact arithmetics could be used).

(2) To improve a little bit this criterion the following has been done. When $|\mathrm{Im}\, x| > M$ we look at $|\mathrm{Re}\, x|$. If this value is less than some large number $N$ (taken as $10^{12}$ in double precision and $10^{28}$ in quadruple) then we look as the value of $\cos(\mathrm{Re}\, x)$. Indeed, the imaginary part of the first component of the next iterate will be $\mathrm{Im}\, x + \mathrm{Im}\, y + \varepsilon \cos(\mathrm{Re}\, x) \cosh(\mathrm{Im}\, x)$. Typically the largest contribution comes from the last term. It will produce a change in the sign of $\mathrm{Im}\, x$ if $\cos(\mathrm{Re}\, x) < 0$. In that case it will be marked white. Otherwise, if $\cos(\mathrm{Re}\, x) \geq 0$, it is marked black. If $|\mathrm{Re}\, x| > N$ then we can not rely on the value of $\cos(\mathrm{Re}\, x)$ and it has been decided (arbitrarily) to leave it as white.

(3) A maximum number of iterates is done for each initial point. If no decision is made on the colour of the pixel when this number is reached, it is left as white. However, in most of the figures, this do not happens for any point on the grid, the maximum number of iterates being taken as $10^6$.

(4) No matter which values of $M$ and $N$ are used there will be points which are marked in the wrong colour. In the figures there are areas seen as black

when really the white points are dense in them. The same happens with the white areas when we plot the ferns corresponding to a number of jumps (crossings through zero of $\operatorname{Im} x$) different from zero. They really contain lots of black points. Finally there are some structures which seem to show up in the ferns that are due to the fact we use a discrete grid in the computations. They can be considered as an optico–geometrical effect.

We discovered experimentally that the tips of the lines which constitute the ferns, are nothing else than homoclinic points.

## 5. Foliations

Now we are going to give a theoretical explanation to this observation. To do that, it is necessary to consider the pure imaginary version of the SM, *i.e.*, the restriction of the complexified standard map onto the purely imaginary part of the complexified phase space.

If we put $x = iX$ , $y = iY$ in the equations (2), this results in the following equations, giving the mentioned purely imaginary version, $SM_{\mathrm{Im}}\colon (X,Y) \mapsto (X_1, Y_1)$ of the standard map:

$$
\begin{aligned}
SM_{\mathrm{Im}}(X,Y) &= (X_1, Y_1), , \\
X_1 &= X + Y_1 , \\
Y_1 &= Y + \varepsilon \sinh X ,
\end{aligned}
\tag{11}
$$

the variable $(X,Y)$ ranging in the real domain $\mathbb{R}^2$.

The following statements are true (see [LP]):

(I) The unstable manifold of the origin of the map (11),

$$
W^u_{\mathrm{Im}} = \left\{ (X,Y) \in \mathbb{R}^2 \colon SM^n_{\mathrm{Im}}(X,Y) \longrightarrow (0,0) , \quad \text{as}\, n \to -\infty \right\} ,
$$

is an analytical smooth curve which has 1-to-1 projection onto the $X$-axis. If we write its equation as $Y = g(X)$ then $\lim_{X\to\pm\infty} \frac{g(X)}{X} = 1$ .

(II) For the points $(X,Y) \in \mathbb{R}^2 \setminus W^u_{\mathrm{Im}}$ the backward iterates, $(X_{-k}, Y_{-k}) = SM^{-k}_{\mathrm{Im}}(X,Y)$, tend to infinity in such a way that $\lim_{k\to+\infty} X_{-k} = \pm\infty$. There exists the *unstable to infinity* direction, $\vec{e}^{\,u}(X,Y) = (\cos\alpha^u(X,Y), \sin\alpha^u(X,Y))$, defined by the following convergent continued fraction

$$
\cot \alpha^u(X,Y)) = 1 + \cfrac{1}{\varepsilon \cosh X_{-1} + \cfrac{1}{1 + \cfrac{1}{\varepsilon \cosh X_{-2} + \cdots}}} .
\tag{12}
$$

This follows easily from the fact that the invariance of the foliation gives the relation

$$
\cot \alpha^u(X_{-k}, Y_{-k})) = 1 + \frac{1}{\varepsilon \cosh X_{-k-1} + \frac{1}{\cot \alpha^u(X_{-k-1}, Y_{-k-1}))}} .
$$

The field of directions $(X,Y)\mapsto \vec{e}^u(X,Y)$ can be integrated to the *unstable foliation to infinity*, which is a $\mathcal{C}^\infty$ foliation of the set $\mathbb{R}^2\backslash W^u_{\rm Im}$. If we add $W^u_{\rm Im}$ to this foliation, we loose smoothness. So $W^u_{\rm Im}$ can be considered as a singular leaf of the unstable foliation to infinity. This foliation is displayed in figure 6. The computation of the vector field uses (12) until no changes occur (using a given arithmetics) when introducing a new quotient. Then, it is integrated numerically.

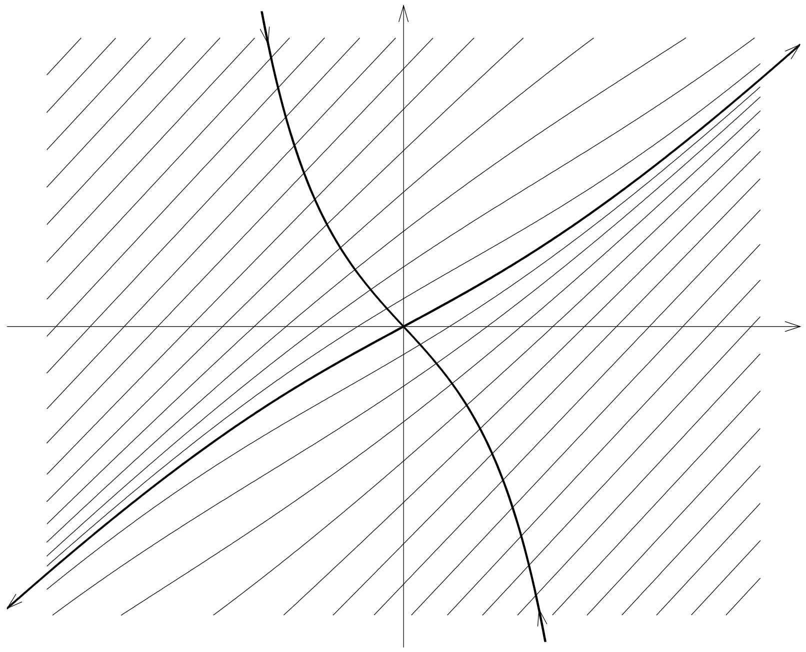

**Figure 6.** The phase portrait of $SM_{\rm IM}$. The unstable foliation to infinity. We have used $\varepsilon=0.5$ and the window $[-8,8]\times[-6,6]$. $W^u$ and $W^s$ are also displayed.

(III) Let us consider the domain of $SM_{\rm Im}$ as the purely imaginary part of the complexified phase space, $S^{\mathbb{C}}=\mathbb{C}^2/2\pi\mathbb{Z}^2$, of the SM, the variables $(X,Y)$ playing the role of local coordinates, the map $SM_{\rm Im}$ being the restriction of $SM$ onto that part. Then all the above constructed objects become immersed into $S^{\mathbb{C}}$. The $W^u_{\rm Im}$ itself can be extended to a (complex) analytic curve, $W^u$, so do the leaves of the unstable to infinity foliation (the latter follows from the unstable manifold theory, see [Pes2]). The union of the extensions of all leaves is a smooth injectively immersed 3-dimensional manifold which we call the *train* of $W^u_{\rm Im}$ and denote by $\mathcal{T}^u$. Thus, $\mathcal{T}^u$ is foliated into holomorphic curves, each being an immersed image of $\mathbb{C}$. Additionally, one can assert that each one of these curves possesses a unique intersection with $W^s_{\rm Im}$, the stable manifold of $SM^{Im}$ (see figure 6). So the leaves of $\mathcal{T}^u$ can be labeled by points of $W^s_{\rm Im}\setminus(0,0): p\mapsto \mathcal{T}^u_p$. We have

$$\mathcal{T}^u=\bigcup_{p\in W^s_{\rm Im}\backslash(0,0)}\mathcal{T}^u_p\,.$$

The point $(0,0)$ divides $W^s_{\rm Im}$ into two pieces: $W^{s\pm}_{\rm Im}$, the signs $\pm$ being related to the right and left half planes where the corresponding curve lies. This gives a subdivision of the train into the *positive* and *negative trains*:

$$\mathcal{T}^{u\pm} = \bigcup_{p \in W^{s\pm}_{\mathrm{Im}}} \mathcal{T}^u_p\,, \quad \mathcal{T}^u = \mathcal{T}^{u+} \cup \mathcal{T}^{u-}\,.$$

(IV) The application of the reversor $R\colon S^{\mathbb{C}} \to S^{\mathbb{C}}$, which is given in coordinates $(x, y)$ by the equation

$$R\colon \begin{pmatrix} x \\ y \end{pmatrix} \longmapsto \begin{pmatrix} -x \\ y + \varepsilon \sin x \end{pmatrix}, \tag{13}$$

converts unstable manifolds to the stable ones. So we have the stable train

$$\mathcal{T}^s = \bigcup_{p \in W^u_{\mathrm{Im}} \setminus (0,0)} \mathcal{T}^s_p = \mathcal{T}^{s+} \cup \mathcal{T}^{s-}$$

with leaves

$$\mathcal{T}^{s\pm}_p = R\left(\mathcal{T}^{u\mp}_{R(p)}\right)\,.$$

Both manifolds $\mathcal{T}^u$ and $\mathcal{T}^s$ are very tricky. Each of the four manifolds, $\mathcal{T}^{u,s\pm}$, is diffeomorphic to $\mathbb{R}^3$, and it is the image of $\mathbb{R}^3$ with respect to an injective $\mathcal{C}^\infty$ immersion. The complexity of these immersions reflects that of the situation with homoclinics which H.Poincaré told about. To get a simplier object to deal with, we introduce *local trains*:

$$\mathcal{T}^{s\pm}_{loc} = \bigcup_{p \in W^{u\pm}_{\mathrm{Im}} \cap W^u_{loc}} \left[\mathcal{T}^s_p\right]_\delta\,,$$
$$\mathcal{T}^{u\pm}_{loc} = R\left(\mathcal{T}^{s\mp}_{loc}\right)\,,$$

where $W^u_{loc}$ was defined on the Step 1 of the construction of the unstable manifold, and $\left[\mathcal{T}^s_p\right]_\delta$ is a small disk of radius $\delta$ around the point $p$ in the complex curve $\mathcal{T}^s_p$ (we fix a metric in $S^{\mathbb{C}}$). The local train looks like the product of the interval and the complex disk: $I \times D$.

## 6. Real homoclinic points

Now return to the consideration of the picture of ferns drawn on figure 5. Recall that this is, essentially, a picture drawn on the domain $D$ defined by (10). Consider first the "real" tips of the fern, *i.e.* those with Im $z$=0. They correspond to real homoclinic points. In one fundamental domain of the real part of $W^u$, we look at the two "primary homoclinic points" (the ones with all the iterates satisfying $0 < x < 2\pi\,, y > 0$). We define the "first" primary homoclinic point as the one which has an iterate on $x = \pi$, the other being denoted as the "second" homoclinic point. The "main tip" on figure 5 corresponds to the second primary homoclinic point, denoted as $z_2$ on figure 7, the first primary one being denoted as $z_1$. (Here we use, freely, the same notation for the homoclinic point and for the corresponding value in the $z$ variable).

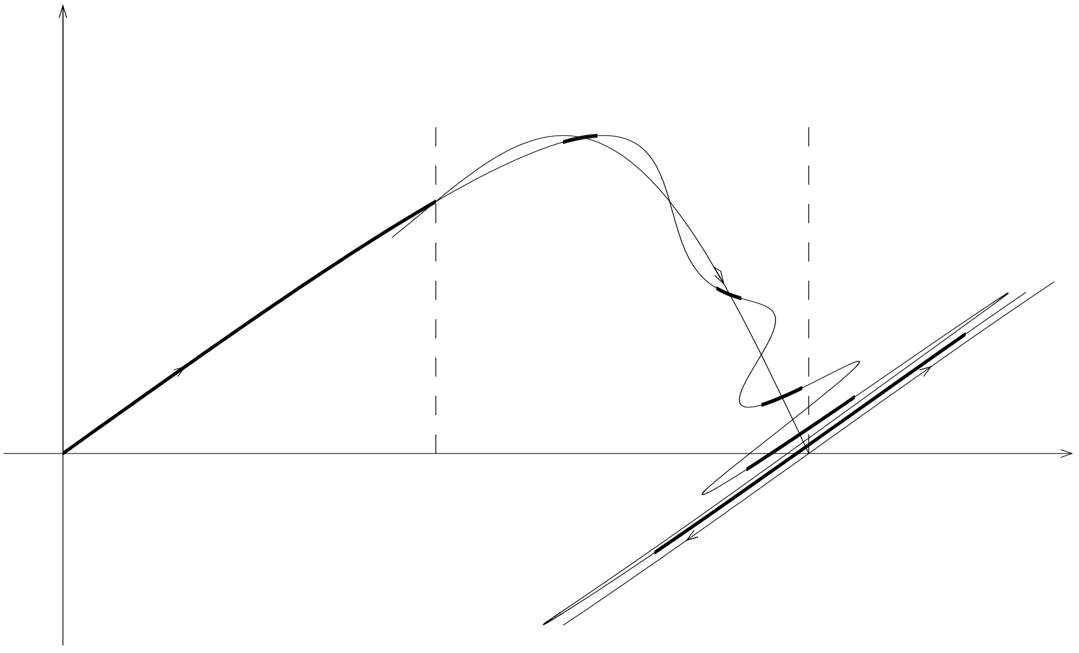

**Figure 7.** A part of the upper halfplane of the phase space of the SM in the real domain with the variable $x$ axis containing the interval $[0, 2\pi]$. A part of $W^u$ described in the text is shown together with the segment $L$, the points $z_1$ and $z_2$, the segment $L_2$ and its images approaching to $W^u_{loc}$, the latter being drawn at the point $x = 2\pi$.

Denote by $L$ the closed arc on $W^u$ joining the origin and the point $z_1$. The segment $SM(L) \setminus L$ contains the second primary point, $z_2$, which belongs also to the arc $R(L) \subset W^s$. Consider a small segment $L_2 \subset SM(L) \setminus L$ with $z_2$ as a center. Its iterates, $SM^n(L_2)$, approach $W^u_{loc}$ as $n \to +\infty$ (see figure 7). So does a small complex neighbourhood, $D_2$, of $z_2$ in $W^u$. The set $SM^n(D_2)$ approaches $W^u_{loc}$ so that it can be embedded in $W^u_{loc}$ as an open neighbourhood of the origin by a transformation which is very close to a small parallel shift. Consider now the local stable train, $\mathcal{T}^s_{loc}$. Since its leaves are transversal to $W^u_{loc}$, it follows that they are transversal to $SM^n(D_2)$ too, and each leaf has an intersection with $SM^n(D_2)$ which consists of only one connected component, provided $n$ is large enough and $L_2$ is small enough. The points of this intersection constitute a one dimensional segment $l_2 \subset W^u$ with the end at the point $SM^n(z_2)$. The segment $l_2$ is a part of the line of the fern on figure 5 which ends at the point corresponding to $z_2$.

To reproduce this more globally, let us turn to the picture, drawn on figure 4 $a$), which represents the plane of the auxiliary variable $\xi$ along $W^u$. Denote by $\xi_2$ the point on this plane which represents $z_2$. The segment $l_2$ looks, in this representation, as a small smooth arc touching transversely the real axis at the point $\xi_2$. Of course, it can be prolonged to a global curve. Denote it by $l$ on the plane of the variable $\xi$. The numerical experiments show that the curve $l$ goes up and approaches the imaginary axis (which corresponds to $W^u_{\mathrm{Im}}$), as it is shown on figure 8 $a$). Recall that the restriction of SM onto $W^u$ looks, in the $\xi$ variable, as the multiplication by $\lambda$. The iterates of SM transform the intersection $W^u \cap \mathcal{T}^{s+}$ into itself because both sets are invariant. Applying multiplication by $\lambda^k$, $k \in \mathbb{Z}$ the curve $l$ produces

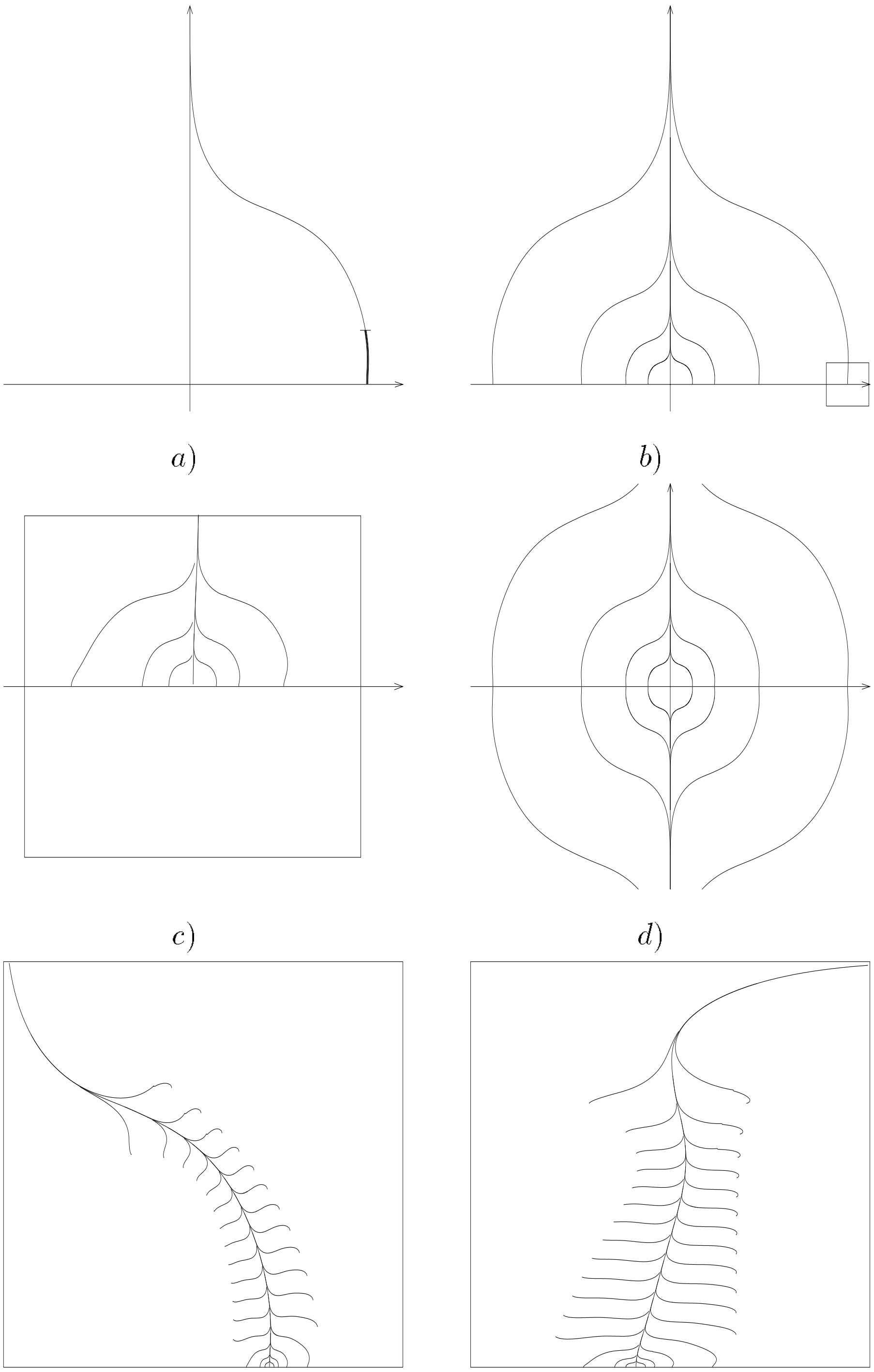

*a*) *b*) *c*) *d*) *e*) *f*)

**Figure 8.** *a*) The curve $l$ in the $\xi$ plane. *b*) The images of $l$ under multiplication by powers of $\lambda$. *c*) A magnification of the square in *b*) showing satellite lines around $l$. *d*) The same as *b*) including the symmetrical part to show the "onion"-like structure. *e*) The main "filament" and some of its secondary branches in the $\xi$ plane. Window: $[0,1]\times[0,1]$. *f*) The same as *e*) in the $\hat{z}$ plane, using the window $[-1,0]\times[0,1]$.

a family of curves drawn on figure 8 *b*). Symmetry reasons lead to the existence of another such family obtained by reflection with respect to the imaginary axis.

We have a pattern which mimics the "secondary lines" of ferns in a neighbourhood of $z_2$. For the convenience of the reader we reproduce here a magnification of such a neighbourhood on figure 9.

We recall that $\mathcal{T}^s_{loc}$ intersects points on $W^u$ represented in the $\xi$ variable as a small segment on the positive part of the imaginary axis (see figure 8). Hence, the piece $SM^n(D_2)$ with $n$ large acquires also intersections with parts of $\mathcal{T}^{s+}$ which are neighbourhoods of points of the lines $\lambda^{-k}l$ with endpoints at the points $\lambda^{-k}\xi_2$ drawn on figure 8 $b$). The whole of this picture is reprinted on $SM^n(D_2)$ and hence on $D_2$. This gives the secondary lines of figure 9, with ends at the points $z_{2,k}$, the "secondary" real homoclinic points around the second primary one.

To obtain the "ternary" lines one has simply to iterate this procedure, that is to apply it to the secondary homoclinic points $z_{2,k}$. This gives a picture which is zoomed and displayed on figure 8 $c$). The iteration of the described procedure gives a complicated picture of lines with ends at real homoclinical points which is similar to the one shown on figure 9.

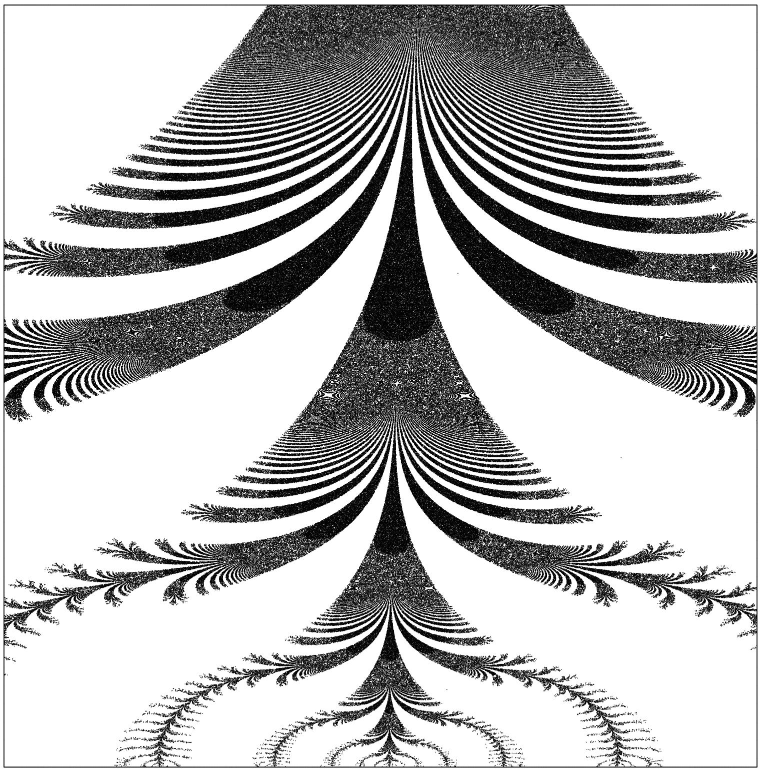

**Figure 9.** A magnification of figure 5. Domain of $\hat{z}$ : $[-0.591, -0.581] \times [0, 0.01]$.

## 7. Itineraries and filaments

Let us consider a value of the parameter $\hat{z}$ of $W^u$. We can compute the corresponding point on the phase space and obtain its orbit by iteration. To any orbit we can associate an *itinerary* as follows: Let $(x_k, y_k)$ be the successive points on the orbit. They will be considered in $\mathbb{C}^2$, that is, without taking modulus $2\pi$ for the reals parts of $x$ and $y$. For definiteness we assume that the one corresponding to $\hat{z}$ has index $k=0$. Given a point of the orbit we assign a number to it: $i_k = \frac{E[\mathrm{Re}\, x]-\pi}{2\pi}$, where $E[\,]$ denotes the integer part. Then the *itinerary* of the orbit is the sequence $(i_0, i_1, i_2, \cdots)$. We shall also use the notation $((i_a)^{k_a}\,(i_b)^{k_b}\,(i_c)^{k_c}\,\cdots)$ for an itinerary consisting of $i_a$ repeated $k_a$ times, followed by $i_b$ repeated $k_b$ times, then by $i_c$ repeated $k_c$ times, etc. The notation $(i_a)^\infty$ is also evident, and it can appear only as last term in the itinerary.

The definition of the itinerary for a point in $W^u$ depends on the value of $\delta$, the radius of the disk where the $\xi$ variable ranges. When $\delta$ decreases to zero we are adding a string of -1 to the left. Hence, we have to talk about $\delta$-itineraries, because $\delta$ must be specified. Equivalently we can specify the initial domain of $\hat{z}$. But, if there is no possible confusion we shall assume $\hat{z}$ always in $[-1,0)\times[0,1]$ (corresponds to $\delta=1$) and we shall not specify $\delta$. With this assumption the value of $i_0$ is always -1 or 0. This is achieved by taking the expansion in (5) up to a suitable order.

A practical question is that, for a given orbit, we shall only be able to compute a finite number of points, mainly because of the escape.

From now on we shall restrict ourselves to the zero jumps case (i.e., no changes in $\mathrm{Im}\, x$ during the iterations), despite we can also study the other cases. Consider now a given itinerary of the form $((i_a)^{k_a}\,(i_b)^{k_b}\,(i_c)^{k_c}\,\cdots\,(i_m)^\infty)$. The set of points in $W^u$ with this itinerary will be called a *filament.* For instance, the "main" filament in figure 5, ending on the reals at the second primary homoclinic point, which is equivalent to the arc $l$ in figure 8 $a$), corresponds to an itinerary of the form $((-1)^{k_{-1}}\,(0)^\infty)$. The value of $k_{-1}$ depends on $\delta$ and is, in some sense, irrelevant.

There are simple rules to obtain the itineraries of other filaments. When a part of the fern "detaches" from the main filament (we can call it a "secondary branch") is does so at some level. The level tells us how many times 0 will appear in the itinerary after $(-1)^{k_{-1}}$. The value following the string of zeros tells us if the branch goes to the right (a positive value) or to the left (a negative one), and the number of the branch counted from the central one. The main filament of this branch is of the form $((-1)^{k_{-1}}\,(0)^{k_0}\,(j)^\infty)$, where $j$ is the number of the branch. Similar rules hold for the successive branches. Each time a branch detaches from the current one, there is a variation in the itinerary, jumping by $m$ from the current branch, if the detached branch is the number $m$ with respect to the current one taken as the 0 branch.

In the figure 8 $e$) and $f$) some filaments are displayed, in the $\xi$ and $\hat{z}$ variables, respectively. The ones given here are, beyond the main filament, those with itinerary $((-1)^{k_{-1}}\,(0)^{k_0}\,(j)^\infty)$ with $k_0 = 1, \ldots, 16$ and $j=\pm 1$. The value of $k$ decreases from top to bottom. The ones to the right (resp. left) of the main filament correspond to $j=1$ (resp. $j=-1$).

The set of filaments having the same part of the itinerary, $(i_0, i_1, i_2, \cdots, i_n)$ up to the position number $n$ is called an *n-bouquet.* For instance, the figure 9 contains most of the bottom of the 19-bouquet with initial part of the itinerary equal to $((0)^{19})$. A bouquet is made by a bundle of filaments. In fact, the "leaves" of the ferns are not properly leaves (i.e., planar regions having some positive area) but bouquets. The figure 10 shows parts of several bouquets, obtained by magnification of different parts of figure 9.

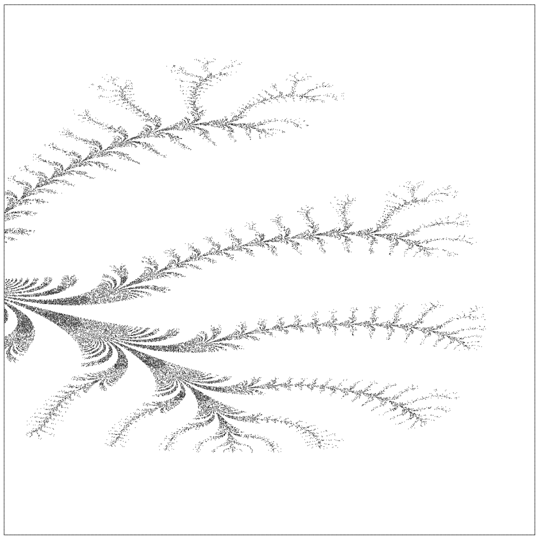

*a*)

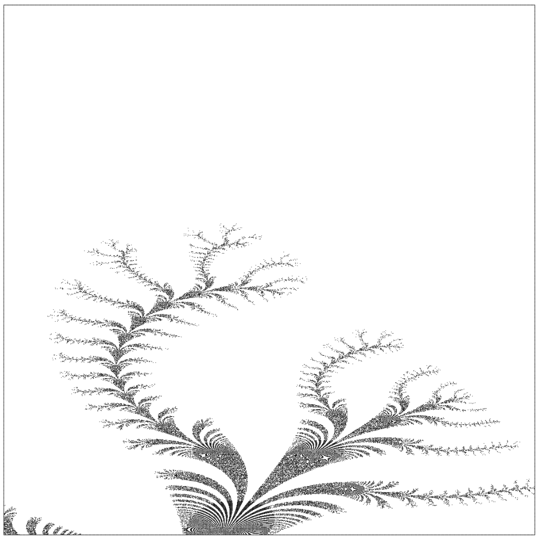

*b*)

**Figure 10.** Magnifications of figure 9: *a*) the window in $\hat{z}$ is $[-0.58235, -0.58225] \times [0.00018, 0.00028]$ and contains the end of the bouquet $((0)^{19}(1)^{12}(2)^{11})$; *b*) the window is $[-0.582317, -0.582316] \times [0.000268, 0.000269]$ and contains the end of the bouquet $((0)^{19}(1)^{12}(2)^{11}(3)^{11}(4)^{10}(5)^{11})$.

The filaments having an itinerary with a very large jump as last jump (for instance, $((0)^{25}\,(-1)^{13}\,(1,000,000)^{\infty}))$ seem to have the last branch very short. Hence, we can state the

**Conjecture 1** The "tips" of the filaments are dense in the fern.

Furthermore, this jump in the itinerary can give rise to a change of sign in $\mathrm{Im}\, x$. This suggest the

**Conjecture 2** Any point in $W^u$ escaping to infinity after $m$ changes of sign of $\mathrm{Im}\, x$, is limit of other points escaping to infinity after $n$ changes of sign for any $n > m$.

Finally, a characteristics of the main filament, with itinerary $((-1)^{k_{-1}}\,(0)^{\infty})$, is that the values of $\mathrm{Re}\, x$ (except for the $k_{-1}$ initial ones) are not only contained in $[\pi, 3\pi]$ but they increase monotonically to $2\pi$. This is useful to obtain figure 8.

## 8. Detection of complex homoclinic points

Let us add to the pictures of the previous two sections the points of intersection with $\mathcal{T}^{s-}$. The analogous procedure will produce a pattern which is the symmetric, with respect to the real axis, of the obtained one. This produces the "onion" like picture drawn on figure 8 *d*). This gives us a method of detecting homoclinic points in the complex domain. Drawing the points escaping to $+\infty$ and to $-\infty$ in the imaginary directions via the positive iterates of the SM produces, in a neighbourhood of such a point, an onion like picture, the "upper half" of the onion being created by points escaping to $+\infty$, the "lower" one corresponding to $-\infty$. In the

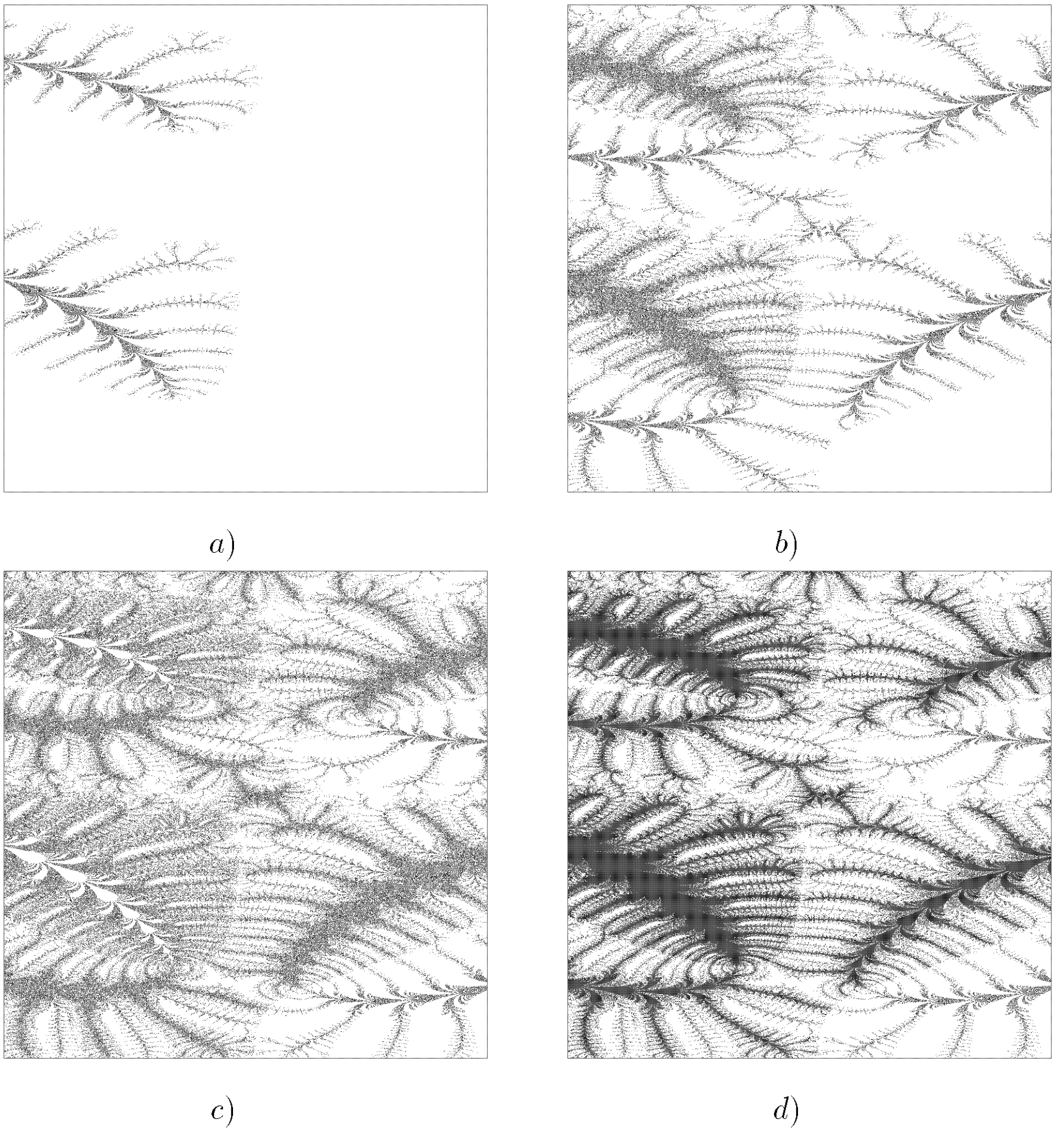

**Figure 11.** In $a)$ , $b)$ and $c)$ the points of $W^u$ with 0, 1 and 2 jumps, respectively, are drawn. $d)$ is the union of the previous three pictures. $\varepsilon = 0.49$ . Window in $\hat{z}$ : $[-0.38, -0.25] \times [0., 0.13]$ .

figures the meaning of "upper" and "lower" depends on the position of the leaves of the fern.

This effect is shown for $\varepsilon = 0.49$ on figures 11 a), b), c) and d), where on the same small region in $D$ given by the inequalities $-0.38 \le \mathrm{Re}\,\hat{z} \le -0.25$ , $0 \le \mathrm{Im}\,\hat{z} \le 0.13$ , are drawn consecutively: a) the points such that the imaginary part of the first component goes to $+\infty$ remaining positive under the positive iterates of the SM (the same as on figures 5 and 9); b) the points such that the imaginary part of the first component of the iterates changes sign once and escapes to $-\infty$ ; c) the points such that the said imaginary part changes sign twice and escapes to $+\infty$ ; d) the superposition of figures a),b) and c). According to Conjecture 2 the closure of b) contains a) and the closure of c) contains both a) and b).

One can see on figure 11 d) the onion like structures surrounding complex homoclinic points.

Returning to figure 7, one can clearly see the reason why the point $z_1$ does not generate ferns on figure 5. This is because we counted only the points whose iterates go to infinity keeping the imaginary part of the first component always positive. But this is not the case for the points belonging to a small disk $D_1$ in $W^u$ surrounding $z_1$. During the first iterates the imaginary part of the first component of the point corresponding to the domain $D_1 \cap D$ is positive because of the definition of $D$. After some iterates it becomes negative, because the iterates of $D_1$ approach $W^u_{loc}$ with a *reversion* of the orientation. After an infinite number of iterates some of the points in $D_1$ escape to infinity. Hence, the imaginary part of the first component tends to $-\infty$. The point $z_1$ becomes visible through the ferns if one switches on the procedure which marks in black the points with the behaviour just described, that is, marking the points whose orbits have exactly one change of sign in the imaginary part of the first component (see figure 12 in [GLST]).

If one changes the parameter $\varepsilon$ of the map, real homoclinic points can bifurcate through a homoclinic tangency to give rise to a pair of complex homoclinic points, and vice versa. This phenomenon is shown on figure 12 which represents both the pictures of $W^s$ and $W^u$ on the real phase space, and the corresponding ferns (in the sense of figure 5) on the complex unstable manifold.

We remark that the first tangency between $W^u$ and $W^s$ is a quadratic one, as can be seen on figure 12 A, but the second one is a cubic one. This is due to the existence of a reversor. As figure 12 B shows, the tangencies are seen using a different number of jumps: 1 (0) in the quadratic (resp. cubic) case. Note that in the right part of figure 12 B, the tip of the main line seems to be the first point of the fern reaching the real axis. This is not true in the left part, where the real axis is first reached by secondary and higher order tips.

It would be possible also to follow the real homoclinic points to the complex ones by a continuation method, following them up to the tangency (going back in $\varepsilon$) and analyzing the bifurcation. This is elementary, but they must be followed individually for each one of the homoclinic points.

## 9. The semistandard map

Consider now the behaviour of the iterates of the SM for large positive values of $\operatorname{Im} x$. By the Euler formula,

$$\sin x = \frac{\mathrm{e}^{ix} - \mathrm{e}^{-ix}}{2i} = \frac{1}{2} i \mathrm{e}^{-ix} + \mathcal{O}\left(\mathrm{e}^{ix}\right) ,$$

the change of variables

$$\begin{aligned} x &= -i \log\left(\frac{\varepsilon}{2}\right) + iu \,, \\ y &= iv \end{aligned} \tag{14}$$

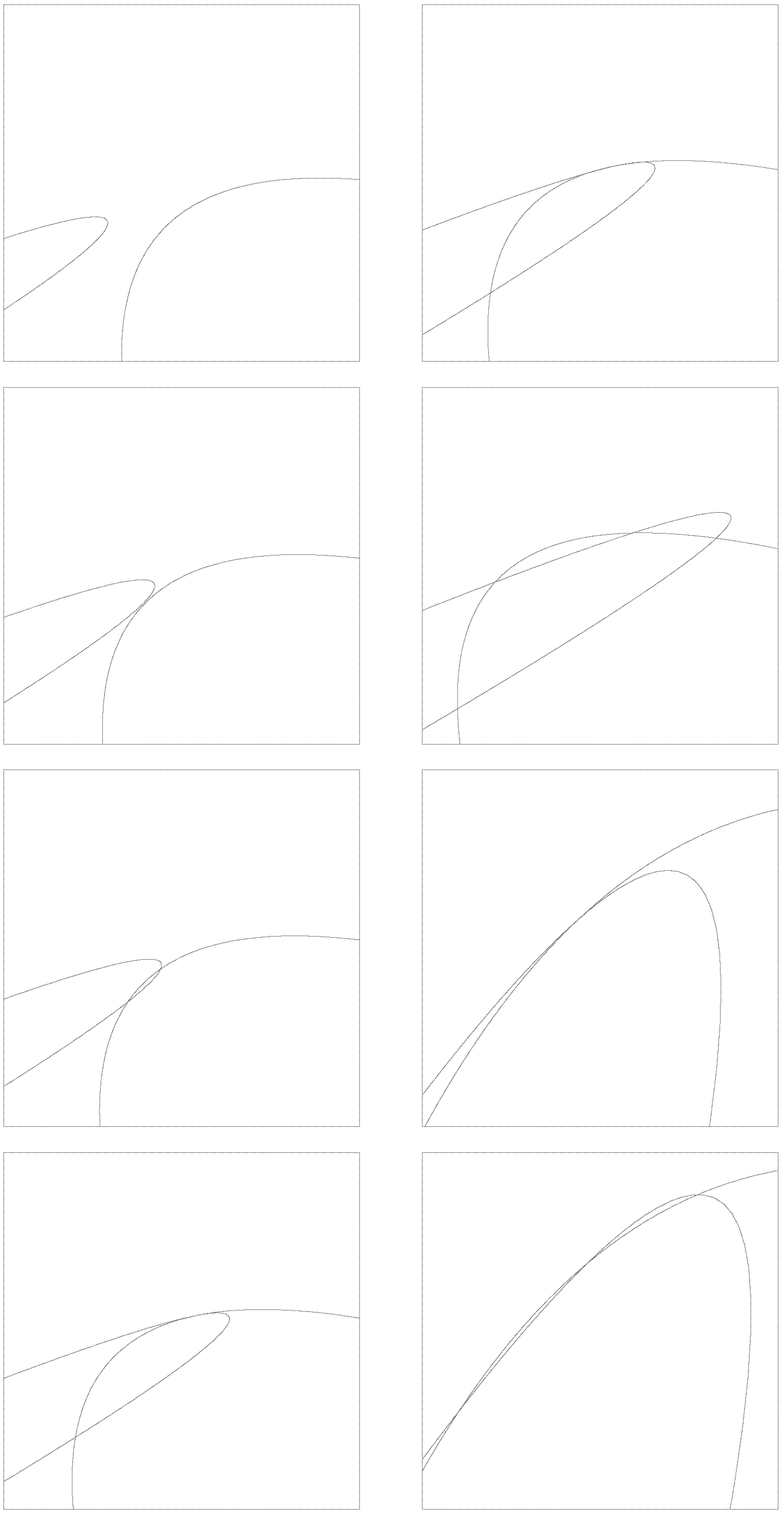

**Figure 12 A.** Several pictures with separatrices: Left, from top to bottom, corresponds to the values of $\varepsilon = 0.491, 0.4917, 0.4918, 0.4928$ in the window $[0.050, 0.057]^2$ of the real phase space of the SM. Right, from top to bottom, the values of $\varepsilon = 0.4929, 0.4940$, in the same window, and $\varepsilon = 0.4928, 0.4929$ in the window $[0.0527, 0.0547] \times [0.0534, 0.0540]$.

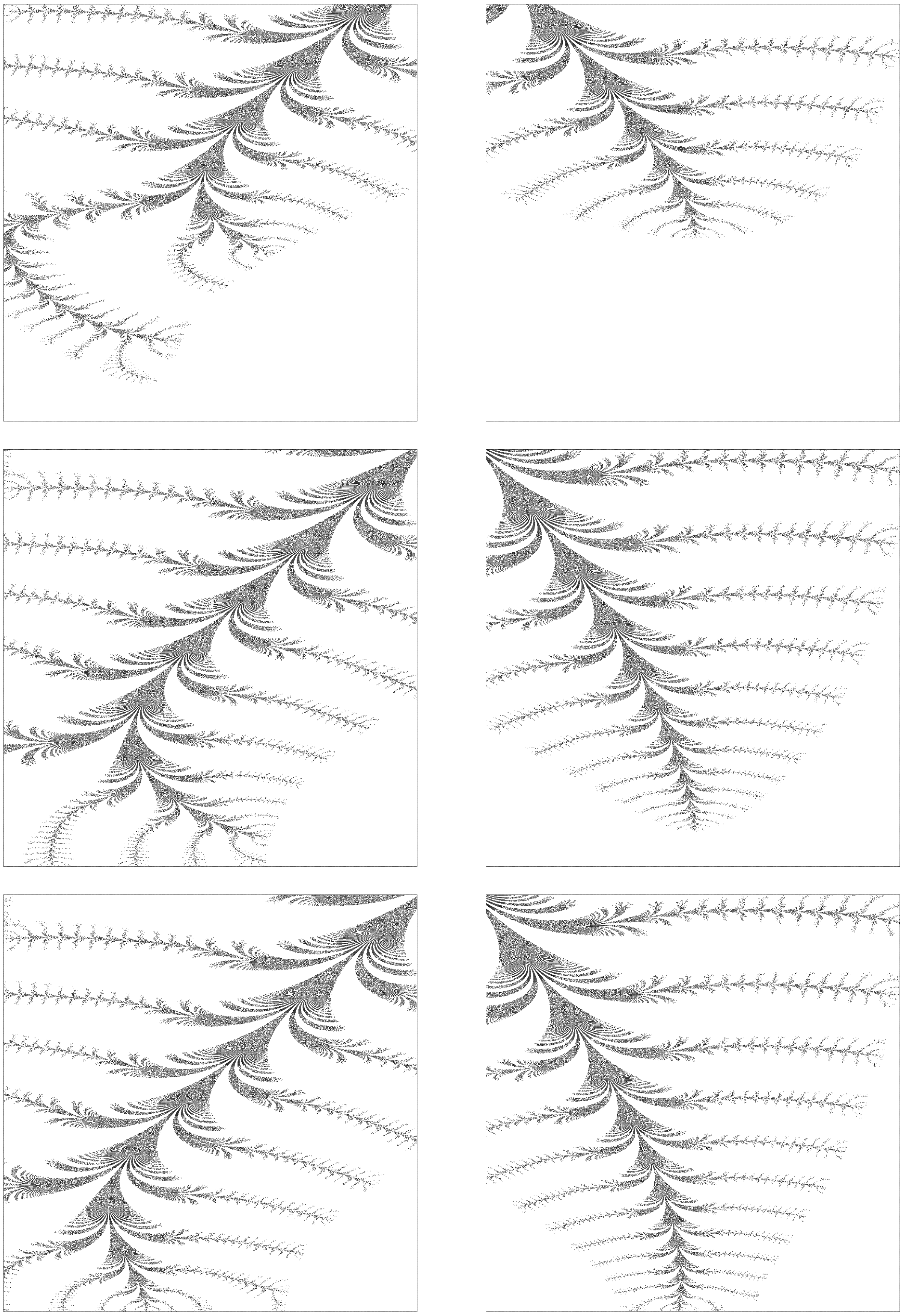

**Figure 12 B.** Pictures of ferns on $W^u$ in the domain of the variable $\hat{z}$: Left, from top to bottom, $\varepsilon = 0.491, 0.4917, 0.4918$ in the domain $[-0.32, -0.29] \times [0.0, 0.03]$, with number of jumps equal to 1. Right, from top to bottom, $\varepsilon = 0.492, 0.4928, 0.4929$ in the domain $[-0.35, -0.32] \times [0.0, 0.03]$, with number of jumps equal to 0.

converts the SM to the form

$$
\begin{aligned}
(u, v) &\longmapsto (u_1, v_1)\,,\\
u_1 &= u + v_1\,,\\
v_1 &= v + \mathrm{e}^{u} - \frac{1}{4}\varepsilon^2 \mathrm{e}^{-u}\,.
\end{aligned} \tag{15}
$$

For large values of $\operatorname{Re} u$, the map (15) can be approximated by the *semistandard* map , SSM (see [Per]), given by the equations:

$$
\begin{aligned}
(u, v) &\longmapsto (u_1, v_1)\,,\\
u_1 &= u + v_1\,,\\
v_1 &= v + \mathrm{e}^{u}\,.
\end{aligned} \tag{16}
$$

The phase space of the SSM is the *complex torus,* $\mathbb{T}^2_{\mathbb{C}} = \mathbb{C}^2 / (2\pi i \mathbb{Z})^2$ .

Define the *fern,* $\mathfrak{F}$, of the SSM as the set of all points $(u, v) \in \mathbb{T}^2_{\mathbb{C}}$ with the real part of the first component escaping to $+\infty$ under the forward iterates of the SSM:

$$
\mathfrak{F} = \left\{ z \in \mathbb{T}^2_{\mathbb{C}}\colon \operatorname{Re} u_n \longmapsto +\infty \quad \text{as} \quad n \to +\infty\,,\ z = (u, v)\,,\ SSM^n(z) = (u_n, v_n) \right\}\,.
$$

Taking into account the relations (14) to (16) one can make the following

**Conjecture 3** The fern $\mathfrak{F}$ of the SSM gives an approximation to pictures like the one drawn on figure 5 for a deep imaginary region in the phase space of the SM.

The complex torus, $\mathbb{T}^2_{\mathbb{C}} = \mathbb{C}^2 / (2\pi \mathbb{Z})^2$ , can be represented topologically as the product $\mathbb{T}^2_{\mathbb{C}} = \mathbb{R}^2 \times \mathbb{T}^2$ by considering $(u, v) \in \mathbb{T}^2_{\mathbb{C}}$ as $(u, v) = (u' + iu'', v' + iv'')$, $u', v' \in \mathbb{R}$, $u'', v'' \in \mathbb{T}^1$, and sending $(u', v')$ to $\mathbb{R}^2$ and $u''$, $v''$ to $\mathbb{T}^2$, the real torus.

Fixing a point $(u', v') \in \mathbb{R}^2$, one gets a *toroidal slice,* $\{(u', v')\} \times \mathbb{T}^2$, in $\mathbb{T}^2_{\mathbb{C}}$. The figure 13 represents the points of the intersection of $\mathfrak{F}$ with several toroidal slices. The figures are symmetric with respect to the point $(\pi, \pi)$ because the escape properties of complex conjugate points are the same. The pixels are marked in black if for some iterate of the corresponding point one has $u' > 700$ unless $u'' < 10^{12}$ and $\cos u'' < 0$. The escape criteria given in section 4 of [GLST] have been used to decide that a pixel is marked in white.

The fern $\mathfrak{F}$ contains the "main" sheet which is the train of the unstable manifold $\Gamma_{-,\mathbb{R}}$ to $-\infty$. One can prove (see [L1,L2]) that there exists an analytic, invariant with respect to the SSM, curve $\Gamma^u \subset \mathbb{T}^2_{\mathbb{C}}$ which is the image of $\mathbb{C}$ under an injective analytic immersion $x \mapsto (u(x), v(x))$, such that

(1) the said immersion conjugates the restriction of the SSM onto $\Gamma^u$ with the shift $x \mapsto x + 1$;
(2) the function $u(x)$ has the following asymptotics in a sector $\delta < \arg x < 2\pi - \delta$, $\delta > 0$:

$$
u(x) = -\log \frac{x^2}{2} + \mathcal{O}\left(\frac{1}{x^2}\right)\,, \tag{17}
$$

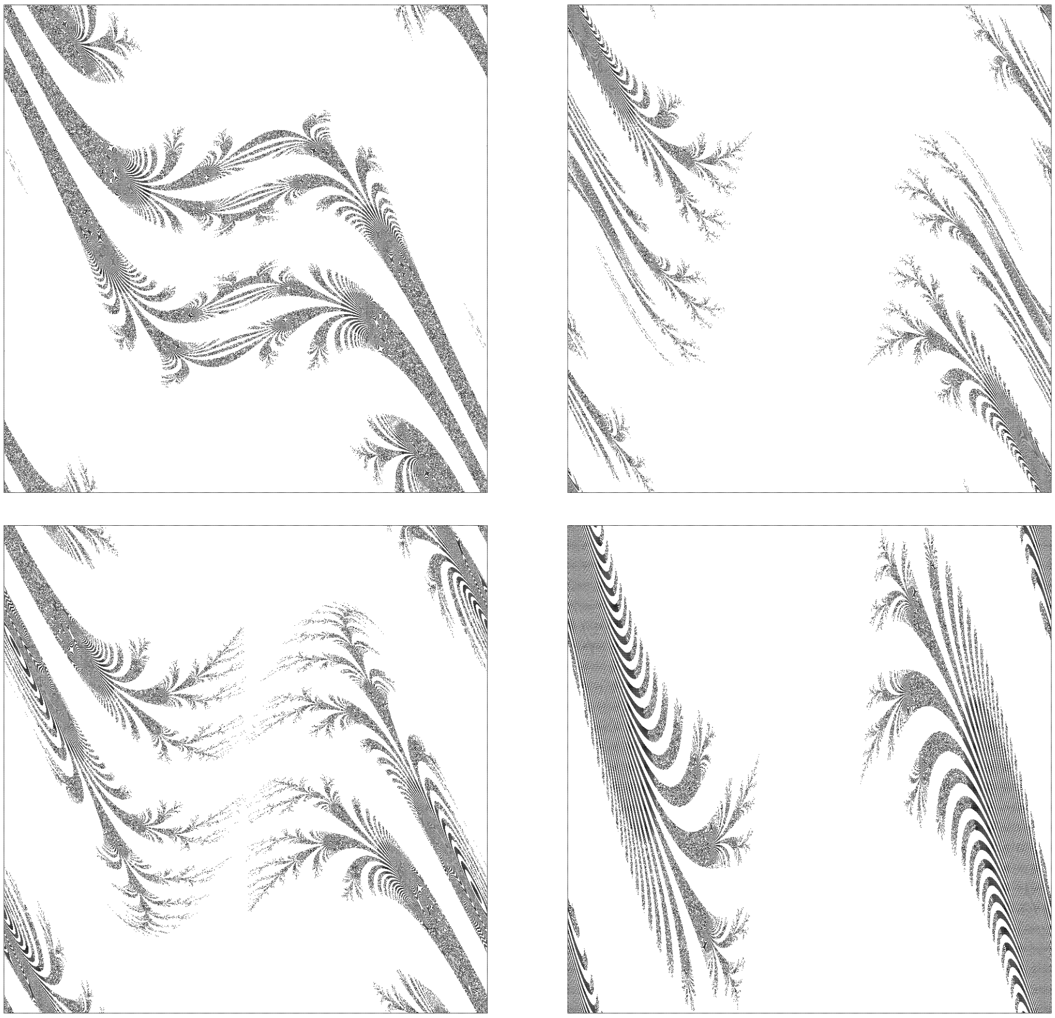

**Figure 13.** Several toroidal slices of the fern of the SSM. The corresponding values of $(u', v')$ are: left top $(0., 1.)$, left bottom $(0., 0.515)$, right top $(0., 0.)$, right bottom $(1., 1.)$. In all the cases the window for $u''$, $v''$ is $[0., 2\pi] \times [0., 2\pi]$.

$\log \frac{x^2}{2}$ being real if $x$ belongs to the negative part of the real axis. See the Appendix A.2 in [GLST] for the computation of coefficients in (17). The expression of $v(x)$ is obtained from the one of $u(x)$ by means of

$$v(x) = u(x) - u(x-1)\,.$$

The immersion is defined uniquely by the properties (1), (2).

The application of the reversor given by the equations:

$$\hat{R}\colon \begin{pmatrix} u \\ v \end{pmatrix} \longmapsto \begin{pmatrix} u \\ -v - \mathrm{e}^u \end{pmatrix},$$

converts $\Gamma^u$ to the stable to $-\infty$ manifold $\Gamma^s$. (In the papers [L1,l2] these curves were designated as $\Gamma_-$ and $\Gamma_+$ correspondingly.) Consider the real part of the phase space, namely $\mathbb{R}^2 \subset \mathbb{T}^2_{\mathbb{C}}$, consisting of points $(u, v)$ with real $u$ and $v$. Define the *real parts* of the stable and unstable manifolds as their intersections with $\mathbb{R}^2$: $\Gamma^u_{\mathrm{Re}} = \Gamma^u \cap \mathbb{R}^2$ and $\Gamma^s_{\mathrm{Re}} = \Gamma^s \cap \mathbb{R}^2$. They are shown on figure 14.

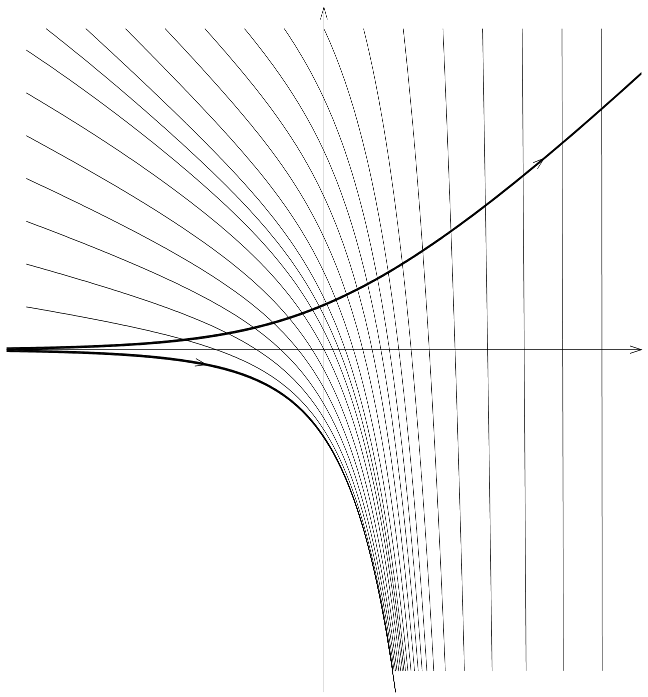

**Figure 14.** Real parts of the invariant manifolds of the SSM. The stable foliation to infinity is also displayed above the stable manifold. Window $[-8,8] \times [-8,8]$.

In the same manner as in the case of the SM, we can show that, in the domain above $\Gamma^s_{\mathrm{Re}}$, there exists the field of the stable to $+\infty$ directions which can be integrated to the stable foliation. The leaves of this foliation can be extended analytically and constitute the stable train:

$$\mathcal{T}^s = \bigcup_{p \in \Gamma^u_{\mathrm{Re}}} \mathcal{T}^s_p .$$

If we add to $\mathcal{T}^s$ the "singular" leaf $\Gamma^s$, we obtain the *completed stable train* $\hat{\mathcal{T}}^s = \mathcal{T}^s \cup \Gamma^s$. Topologically $\hat{\mathcal{T}}^s$ is the image under an injective continuous map of $\mathbb{R}^3_+ = \{(x,y,z) \in \mathbb{R}^3 \colon x \geq 0\}$. The mentioned map can be chosen to be a smooth immersion in interior points of $\mathbb{R}^3_+$, and analytic with respect to the last two coordinates if one uses the representation $\mathbb{R}^3_+ = \mathbb{R}^1_+ \times \mathbb{C}$. The image of the boundary of $\mathbb{R}^3_+$ is $\Gamma^s$.

The train $\mathcal{T}^s$ is the main sheet of the fern $\mathfrak{F}$, the boundary points looking as sharp tips of the fern on figure 13.

Apart of $\mathcal{T}^s$, the fern $\mathfrak{F}$ contains a lot of other sheets. Its local structure is very complicated: a neighbourhood of a typical point of $\mathfrak{F}$ in $\mathfrak{F}$ contains the product of the Cantor set and a 3-ball. This was proven in [L3]. Here follows a sketch of the proof. The main role is played by the term $\mathrm{e}^u$ in (16) which is large for large values of $\mathrm{Re}\, u$. A point $(u,v)$ belongs to $\mathfrak{F}$ if $\mathrm{Re}\, u$ goes to $+\infty$ under the iterates of the SSM. Due to the second line of (16), this happens if $\mathrm{Re}\, v$ is always positive during the succesive iterations. In its turn, due to the last equation (16), this takes place if $\mathrm{Re}\, \mathrm{e}^u$ is positive, or equivalently, if $\mathrm{Im}\, u \in ]-\frac{\pi}{2}+2k\pi, \frac{\pi}{2}+2k\pi[$, $k \in \mathbb{Z}$. Take a point $p_0 \in \mathbb{T}^2_{\mathbb{C}}$ with large $\mathrm{Re}\, u$ such that $\mathrm{Im}\, u \in ]-\frac{\pi}{2}+2n_0\pi, \frac{\pi}{2}+2n_0\pi[$ for some $n_0 \in \mathbb{Z}$, and consider a small 2-dimensional disk $\hat{D}_0$ around $p_0$. If $\hat{D}_0$ is in general position, its magnitude grows under the application of the SSM and becomes so big that $\mathrm{SSM}(\hat{D}_0)$ contains many intersections with the strips $S_n = \{(u,v)\colon -\frac{\pi}{2}+2n\pi < \mathrm{Im}\, u < \frac{\pi}{2}+2n\pi\}$, $n \in \mathbb{Z}$ (see figure 15).

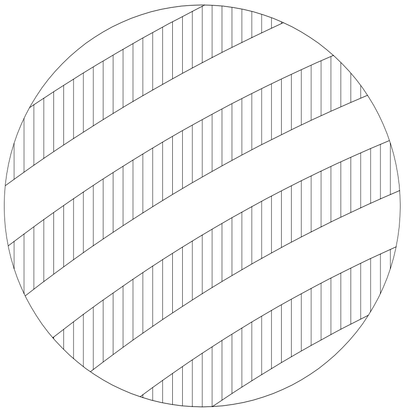

**Figure 15.** Local structure of the fern, in a small disc, at the $n$-th step of the construction.

Choose an integer $n_1$ and construct a disk $\hat{D}_1 \subset S_{n_1} \cap SSM(\hat{D}_0)$. We can repeat the construction again taking $\hat{D}_1$ in place of $\hat{D}_0$ etc. In such a way one can select a sheet of $\mathfrak{F}$ choosing at each step an integer number from some finite but large range of values. It follows that a sheet of $\mathfrak{F}$ has an infinite string, $(n_0, n_1, \dots)$, as a label. The number of such strings in uncountable, and such a process leads to the appearance of the Cantor set.

Returning to the picture on figure 5, it is then natural to make the

**Conjecture 4** Figures like figure 5 contain not only the intersections with $\mathcal{T}^{s,\pm}$, but they contain, also, uncountable many other lines.

Any homoclinic point is the common boundary of $\mathcal{T}^{s+} \cap W^u$ and $\mathcal{T}^{s-} \cap W^u$. Two possibilities are shown on figure 16: a real homoclinic point, $p_0$, and a pair of complex conjugate homoclinic points, $p_1$ and $p_2$. The picture is drawn on the plane of the variable $\xi$ (cf. figure 8). For this picture we have used the value $\varepsilon = 0.49$. The line drawn with a homoclinic point, $p_0$, in the real axis, corresponds to the itinerary $((-1)^{k-1}\,(0)^{14}\,(1)^{\infty})$. The ones with a non real homoclinic point ($p_1$ and $p_2$) have itinerary $((-1)^{k-1}\,(0)^{13}\,(1)^{\infty})$. They are symmetrical the one from the other with respect to the real axis. In the upper curve with this itinerary, the upper part (up to $p_1$) has 0 jumps and the lower part has 1 jump. One can also compare with figure 11 $a$) and $b$).

To make visible the lines $\mathcal{T}^{s,\pm} \cap W^u$ going through a homoclinic point, one should take into account that a point of the train goes to infinity under the iterates of the SM *ultimately*. This means that, according to the type of the homoclinic point, the points of its train can make several crossings of the real axis (their first coordinates) and finally escape to $\pm\infty$.

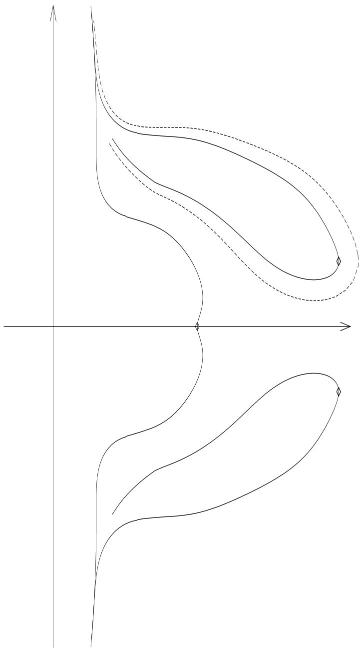

**Figure 16.** Filaments containing real or complex homoclinic points in the $\xi$ plane. $\varepsilon = 0.49$ . Window: $[0.625 : 0.825] \times [-0.15 : 0.15]$ . See additional explanation in the text.

If we select the points with a given number of such crossings, we obtain, in fact, a continuum of curves, a countable number of them containing a homoclinic point. The lines without homoclinic points can not intersect the real axis. One such line is drawn on figure 16 in broken lines.

## 10. The vicinity of the elliptic fixed point

The SM has an elliptic fixed point at $(x, y) = (\pi, 0)$ . The eigenvalues are given by (4) by replacing $\varepsilon$ by $-\varepsilon$ . Let us consider its behaviour in $\mathbb{C}^2/2\pi\mathbb{Z}^2$ . To this end we write $x$ and $y$ as complex variables: $x = \pi + p + i\,q$ , $y = r + i\,s$ , where $p$ and $r$ are taken modulus $2\pi$ and the fixed elliptic point is now at the origin. In these real coordinates the map (2) is written as

$$\begin{pmatrix} p \\ q \\ r \\ s \end{pmatrix} \mapsto \begin{pmatrix} p_1 \\ q_1 \\ r_1 \\ s_1 \end{pmatrix} = \begin{pmatrix} p + r_1 \\ q + s_1 \\ r - \varepsilon(\sin p \cosh q) \\ s - \varepsilon(\cos p \sinh q) \end{pmatrix} . \tag{18}$$

It can be considered as a symplectic map in $\mathbb{R}^4$ with respect to two different symplectic forms simultaneously, $\Omega_{\mathrm{Re}} = dp \wedge dr - dq \wedge ds$ and $\Omega_{\mathrm{Im}} = dp \wedge ds + dq \wedge dr$ , which are the real and imaginary parts of the form $\Omega = dx \wedge dy$ . In $\mathbb{R}^4$ the elliptic fixed point is totally elliptic, the eigenvalues being double, of course. But the degeneracy prevents the existence of KAM tori and, furthermore, the elliptic fixed point is generically unstable.

To prove the instability is enough to consider normal forms around the elliptic point. Letting aside values of $\varepsilon$ leading to resonance, there exists an analytical change of variables from $(x,y)$ to $(X,Y)$ allowing to put the SM (or whatever analytic map we consider) in Birkhoff normal form:

$$\begin{pmatrix} X \\ Y \end{pmatrix} \mapsto \begin{pmatrix} \cos\alpha & \sin\alpha \\ -\sin\alpha & \cos\alpha \end{pmatrix} \begin{pmatrix} X \\ Y \end{pmatrix} + O(|(X,Y)|^{N+1}), \tag{19}$$

for any arbitrary large, but fixed, value of $N$. The angle $\alpha$ can be written as

$$\alpha = \alpha_0 + \alpha_1\rho^2 + \alpha_2\rho^4 + \cdots ,$$

where $\alpha_j$ denote the Birkhoff coefficients and $\rho^2 = X^2 + Y^2$. In the case of the standard map, as $\varepsilon$ is real, the Birkhoff coefficients are real. If we only consider the normal form in (19) then $\rho^2$ is invariant. Going back to real variables it has the expression $\rho^2 = \Gamma + i\,\Delta = (P^2 - Q^2 + R^2 - S^2) + i\,2(PQ + RS)$, where now $X = P + i\,Q$, $Y = R + i\,S$. Substituting in the expression of $\alpha$ we have $\alpha = \gamma + i\,\delta$, where $\gamma$ and $\delta$ depend on the Birkhoff coefficients and on $\Gamma$ and $\Delta$. Hence, they are constant along a given orbit of the normal form.

Let us introduce $c = \cos(\beta)$, $s = \sin(\beta)$, $C = \cosh(\gamma)$, $S = \sinh(\gamma)$. The normal form in (19) can be expressed in real as

$$\begin{pmatrix} P \\ Q \\ R \\ S \end{pmatrix} \mapsto \begin{pmatrix} C & 0 & 0 & S \\ 0 & C & -S & 0 \\ 0 & -S & C & 0 \\ S & 0 & 0 & C \end{pmatrix} \begin{pmatrix} c & 0 & -s & 0 \\ 0 & c & 0 & -s \\ s & 0 & c & 0 \\ 0 & s & 0 & c \end{pmatrix} \begin{pmatrix} P \\ Q \\ R \\ S \end{pmatrix}. \tag{20}$$

As the two matrices in (20) commute and the one containing the trigonometric terms preserves the euclidean norm, it is enough to look at the matrix containing the hyperbolic terms. It has the double eigenvalues $\exp(\pm\gamma)$. The unstable eigenspace is generated by the vectors $(1,0,0,1)^T$ and $(0,1,-1,0)^T$, and the stable one by $(1,0,0,-1)^T$ and $(0,1,1,0)^T$. This behaviour produces the instability: no matter how close to the origin we start, there are points leaving a fixed domain. The same is true for the full map. We note, however, that the closer we are to the elliptic point, the slower the escape is. Indeed, the dominant part in $\gamma$ is $\alpha_1 \times 2(PQ + RS)$. If we start at a distance $d$ from the fixed point, the eigenvalue is $\exp(O(d^2))$. Hence, to reach some finite distance $d$ the number of iterates is of the order of $d^{-2}\log(1/d)$. We remark that to have $\gamma \neq 0$ one should should have some "stable component" different from zero. Indeed, if the components of the usntable and stable vectors, as given above, are $\mu_1, \mu_2, \mu_3$ and $\mu_4$, respectively, then the condition to be satisfied is $\mu_1\mu_4 + \mu_2\mu_3 \neq 0$.

With this instability in mind we have looked at points in $W^u$ approaching the elliptic fixed point in the complexes. The figure 17 shows, in different domains of the variable $\hat{z}$, points whose orbit, before escaping, passes at a distance less than some bound from the elliptic point. This is displayed for the value $\varepsilon = 0.5$. We recall that, for that value of $\varepsilon$ the real $W^u$ passes at a distance of the elliptic point near 1.4. When the distance is further reduced the size of the spots in

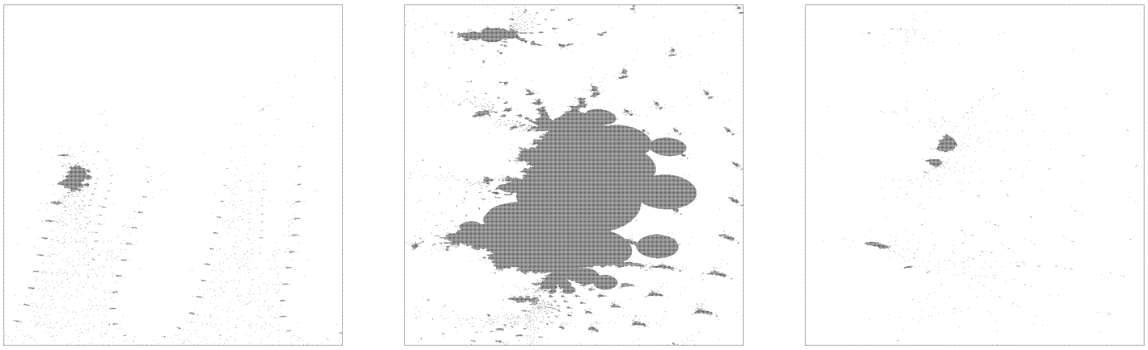

*a*) *b*) *c*)

**Figure 17.** Points in the $\hat{z}$ variable passing at an euclidean distance (in the variables of (18)) less than $d$ from the elliptic point for $\varepsilon = 0.5$: *a*) window $[-1,0]\times[0,1]$, $d=1$. *b*) window $[-0.86,-0.72]\times[0.43,0.57]$, $d=1$. *c*) window $[-0.86,-0.72]\times[0.43,0.57]$, $d=0.5$.

the $\hat{z}$ variable reduces quickly. It is not difficult to locate points of the unstable manifold whose orbits pass at a distance from the elliptic point of the order of $10^{-2}$. A further reduction requires some more work. The figure 18 displays the projection on the real part of the $(x,y)$ variables (i.e., the $(p,r)$ variables) of the orbit corresponding to $\hat{z} = -0.8034907421279 + i\,0.5145580274396$ which reaches a distance to the elliptic point less than 0.00087 (in the euclidean norm). For this 108,063,325 iterates are needed. For comparison the figure shows also the real unstable manifold. To prevent from having the central part of the figure completely black, we have only plotted the iterates whose index is less than or equal to 20,000 modulus 1,000,000. Of course, both the value of $\hat{z}$ and the number of iterates can change slightly depending on the arithmetics.

Using the reversor (13), the $W^s$ also seems to pass as close as desired to the elliptic fixed point when the SM is immersed in the complexes. When an orbit approaches the elliptic fixed point, the real and the imaginary parts of the couple $(x,y)$ have, essentially, a rotational behaviour. This is seen in figure 18, where 20,000 consecutive iterates seem to be on a "curve" (the same is true in the $(q,s)$ projection). The "curve" is slowly shrinking when we continue the iteration. In particular $r = \mathrm{Im}\, x$ changes sign a large number of times.

In fact more seems to be true. We can do the following numerical experiment. Take a lattice of points in the real phase space. For instance 1000 equiespaced points in each of the $x$ and $y$ variables between 0 and $2\pi$. On the other hand, take a large number of points in (a quarter of) the fundamental domain in the $\hat{z}$ variable, iterate them until they eventually escape (or up to a large number of iterates), and, for each one of iterates, record the distance to the closest point in the lattice. At the end, each point of the lattice has an associated distance, so that it is at a distance less than this one from $W^u$. The figures 19 a), b) and c) display in black the points of the real phase space which are (at most) at a distance larger than 0.01, 0.015 and 0.02, respectively, from $W^u$. We note that most of the points in the fundamental domain escape very quickly and just a few of them have the opportunity to approach closely the real phase space before escaping. In the figure

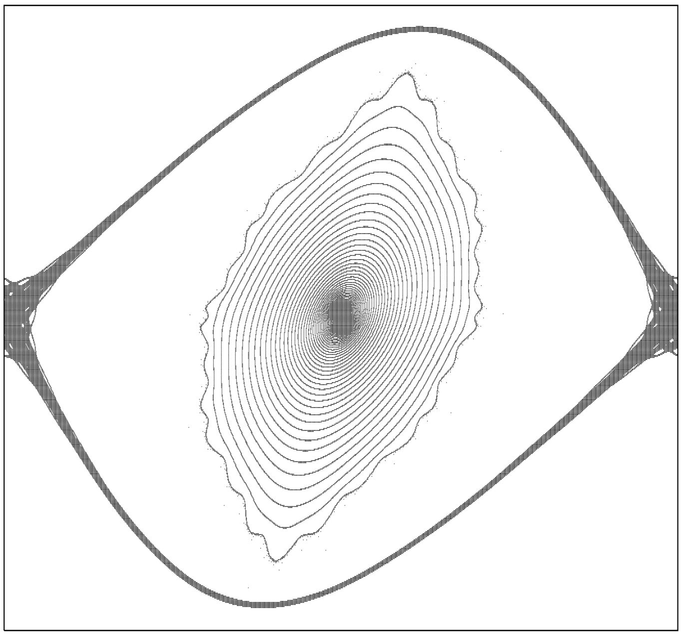

**Figure 18.** The real $W^u$ for the SM and the projection on the real parts of $(x, y)$ of points of an orbit, in the complex $W^u$, which approaches the fixed elliptic point. $\varepsilon = 0.5$. Window: $[0., 2\pi] \times [-\pi/2, \pi/2]$. See additional explanetion in the text.

19a) 76% of the points are in white and, hence, at a distance less than 0.01 from $W^u$. This value increases to 95% and 99.3% in parts b) and c) of figure 19. In the last one we see that only a few points near the elliptic fixed point or in the central region are not so well approximated by $W^u$. If the distance is allowed to increase up to 0.05, only 34 among 1,000,000 points are not close enough to the computed iterates of the complex unstable manifold, and all of them are close to the elliptic one.

Summarizing, we can state the following conjecture:

**Conjecture 5** The closure of the complex unstable and stable manifolds of the standard map contain all the real phase space.

## 11. Final comments and discussion

Finally, let us comment on the result of the following experiment. It is possible to do the same computations presented in figure 5, but marking in black all the point escaping to infinity after an even numbers of crossings of the imaginary axis, or after an odd number of crossings. Even if the number of changes of sign of $\mathrm{Im}\, x$ is limited to 100, this results in almost completely grey figures (and this is the reason why they are not displayed here). The reader can look at figure 11, and have in mind the comments at the end of section 7 (mainly Conjectures 1 and 2), to be convinced about that. The superposition of these two pictures, with even and odd number of jumps, results in a totally black area. At the spots corresponding to a passage close to the elliptic point, as discussed in the previous section, one has to

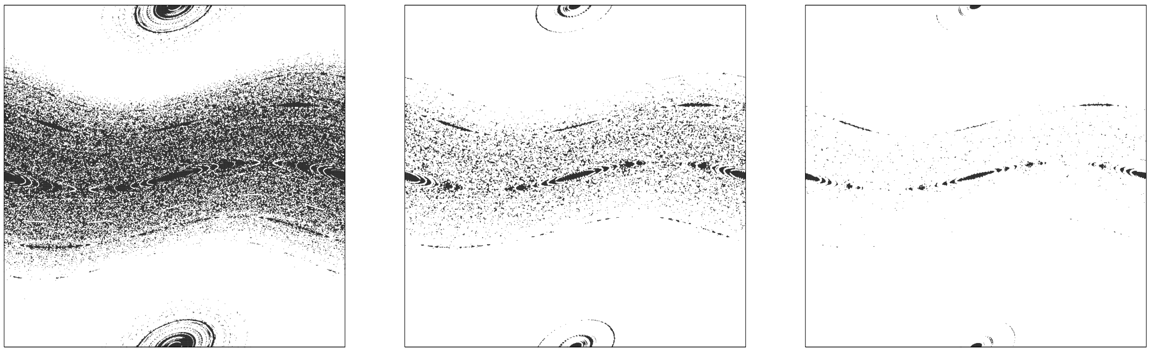

*a*) *b*) *c*)

**Figure 19.** Points in the real phase space of the SM: $(x, y) \in [0, 2\pi] \times [0, 2\pi]$. The points in white are at a distance from the complex $W^u$ less than 0.01 in part *a*), than 0.015 in part *b*), and than 0.02 in part *c*).

wait until the iterates return from a vicinity of that point (eventually they visit this vicinity several times before escaping). This suggests conjectures about the density of "black" objects on $W^u$ . In particular, one can state the

**Conjecture 6** Complex homoclinic points are dense in $W^u$ (and, hence, in $W^s$ ).

The complexity of the real standard map is strongly related to the homoclinic tangle associated to the fixed hyperbolic point. This tangle is evolving with the parameter $\varepsilon$ gaining complexity when the parameter increases, thanks to the creation of "new" real homoclinic points. They are created by homoclinic tangencies which, in turn, are related to the creation of very small stability islands (the conservative version of the Newhouse phenomenon). It turns out that "all" these homoclinic points exist on the complexes for any nonzero value of $\varepsilon$. They "land" on the reals for given values of the parameter. The main difference is that when $\varepsilon$ decreases (resp. increases) the number of secondary branches not touching the real axis (see figures 8 e) or 8 f)) increases (resp. decreases). But, in some sense, the full complexity can be seen in the complex phase space for any nonzero value of the parameter. We believe that this behaviour is common to many families of similar maps, even if they do not have the symmetry properties of the SM, which are due to the reversibility.

**Acknowledgments.** This work was supported by the European INTAS grant 93-0339. The first author also was partially supported by ISF grant R3T000, Grant of the State Higher Education Committee of Russia, and RFFI grant. The second author was also partially supported by the PB94–0215 grant (Spain) and by the European Network Grant ERBCHRXCT 940460. The first version of the paper was written when the first author was a guest in Pennsylvania State University in March–April 1995 and then in Augsburg University in June-July 1995. He thanks professors Katok and Brüning for their hospitality. The second author is indebted to A. Delshams and R. Martínez for helpful suggestions and to J. Timoneda for some printing routines. The computing facilities were provided by grants ESP91–0403 (Spain) and CIRIT GRQ93–1135 (Catalonia).

## REFERENCES

[Ch] B. V. CHIRIKOV, *A universal instability of many–dimensional oscillator systems*, Physics Reports **52** (1979), 263–279.

[GLST] V. G. GELFREICH, V. F. LAZUTKIN , C. SIMÓ , M. B. TABANOV, *Fern-like structures in the wild set of the standard and semistandard maps in* $\mathbb{C}^2$ , International Journal of Bifurcation and Chaos **2, No 2** (1992), 353–370.

[L1] V. F. LAZUTKIN, *Splitting of separatrices for the Chirikov's standard map. Preprint* (1984), VINITI 6372/84.

[L2] V. F. LAZUTKIN, *Exponential splitting of separatrices and an analytical integral for the semistandard map*, preprint, Université Paris VII (1991), 53 p.; *An analytic integral along the separatrix of the semistandard map: existence and an exponential estimate for the distance between the stable and unstable separatrices*, Algebra i Analis **4** (1992), no. 4, 110–142; St.-Petersburg Math. J. **4** (1993), no. 4, 721-748.

[L3] V. F. LAZUTKIN, *Existence of ferns* (June 1993.), Universitat de Barcelona. Mathematics Preprint Series No.137,.

[LP] V. F. LAZUTKIN, M. A. PANKRATOV, *A stable foliation to infinity in the complexified phase space of the standard map* (November 1995.), Universitat de Barcelona. Mathematics Preprint Series No.183,.

[Mo] J. MOSER, *The analytical invariants of an area preserving map near a hyperbolic fixed point*, Commun. Pure Appl. Math. **9** (1956), 673–692.

[Per] I. C. PERCIVAL, *Chaotic boundary of a Hamiltonian map*, Physica D **6** (1982), 67–77.

[Pes1] Ya. B. PESIN, *Lyapunov characteristic exponents and smooth ergodic theory*, Russ. Math. Surveys **32** (1977), 55–114.

[Pes2] Ya. B. PESIN, *Families of invariant manifolds corresponding the nonzero characteristic exponents*, Izvestiya Akademii Nauk SSSR, ser.mat. **40:6** (1976), 1332–1379.

[Po] H. POINCARÉ, , *Les Méthodes Nouvelles de la Méchanique Céleste,*Vols 1–3, Gauthier–Villars, Paris, 1892, reprinted by Dover, New York (1957).

[S] C. SIMÓ, *Analytical and numerical computation of invariant manifolds*, in *Modern methods in celestial mechanics*, D. Benest et C. Froeschlé, editors, Editions Frontières (1990), 285–330.

[1] Physics Department, St.-Petersburg State University, Ulyanov str. 1, kor.1, Petrodvorets, St.-Petersburg, 198904, Russia.
*E-mail address*: lazutkin@onti.phys.lgu.spb.su

[2] Departament de Matemàtica Aplicada i Anàlisi, Universitat de Barcelona, Gran Via 585, 08007 Barcelona, Spain
*E-mail address*: carles@maia.ub.es